The Generation and Propagation of Sea Level Variability Along the Pacific Coast of Mexico

DAVID B. ENFIELD AND J. S. ALLEN

School of Oceanography, Oregon State University, Corvallis, 97331

(Manuscript received 20 September 1982, in final form 1 March 1983)

ABSTRACT

Case history analysis, cross spectra and multiple regression analysis have been used in a study of low-pass filtered sea level records from the Pacific mainland coast of Mexico in 1971 and 1973–75. During the summer–fall season (May–October), sea level variability is characterized by strong alongshore coherence and nondispersive, poleward phase propagation over a wide frequency range (0.02–0.37 cpd). The strength and clarity of the propagating signals seem to be related primarily to large-amplitude events of elevation (10–30 cm) that are generated off the southern coast of Mexico by tropical storms. These events are typically forced by the alongshore, poleward movements of the storms to as far north as 20°N, and thereafter continue to propagate freely at least as far as Guaymas (28°N). Large, variable phase speeds (250–500 km day^{-1}) are observed in the southern region, consistent with the alongshore speeds of the forcing. A multiple-input statistical forcing model, in which adjusted sea level is regressed on local wind, large-scale atmospheric pressure and remote sea level and wind, confirms that the disturbances are forced in the south and propagate freely in the north. North of 20°N, propagation speeds are smaller than in the south and relatively invariant at each station, and show a steady decrease from 250–300 km day^{-1} near Mazatlan (23°N) to 180–230 km day^{-1} near Guaymas (28°N). These characteristics of the northern propagation are consistent with those from the theory of free, linear, hybrid coastal trapped waves, as computed from an inviscid numerical model by Brink (1982). The observed speeds in the south, however, are much faster than predicted by theory, consistent with their forced nature. The model results show a strongly barotropic velocity structure over the continental shelf, and a baroclinic structure farther offshore. In winter (November–April), the alongshore coherence of sea level is less than in summer at all stations, and only appreciable between Acapulco (17°N) and Mazatlan (23°N). The winter phase propagation (140–230 km day^{-1}) is generally slower than in summer, most notably in the south, where it is consistent with a lack of forcing.

1. Introduction

Along low latitude ocean boundaries, baroclinic long waves are a preferred mode of oceanic response to transient wind forcing (e.g., Romea and Allen, 1982). Poleward propagating disturbances with properties similar to those of internal Kelvin waves have been observed equatorward of 15°S along the Peru coast, with frequencies of 0.1–0.5 cycles per day (cpd) (Smith, 1978). The offshore scale of internal Kelvin waves is the internal Rossby radius of deformation δ_R, which decreases with increasing latitude. When a low latitude internal Kelvin wave propagates poleward into a region where δ_R is comparable to the offshore scale of the continental margin, it is theoretically expected to acquire a hybrid form, retaining some of the characteristics of internal Kelvin waves while becoming more like topographically supported continental shelf waves (Allen and Romea, 1980). For typical stratification and offshore topographic scales, this transition should occur in the 10–20° latitude range. Generalized coastal trapped waves in a continuously stratified ocean have been studied by Wang and Mooers (1976), Clarke (1977) and Huthnance (1978). Brink (1982) recently used a numerical model based on the previous work to show that the propagating disturbances observed along the Peru coast fall into this hybrid category. The forcing of such waves within the coastal waveguide has not been observed and is one of the questions prompting ongoing research.

Our work was partly motivated by that of Christensen *et al.* (1983), who have documented a remarkable example of propagating sea level variability along the Pacific coast of Mexico. They find high lagged correlations amongst mainland sea level stations from Acapulco (17°N) to Guaymas (28°N), while stations in this region are uncorrelated with Salina Cruz (16°N) or with stations on either side of the Baja California peninsula. From correlation analysis they determine poleward propagation speeds that increase from 2.2 m s^{-1} (190 km day^{-1}) near Acapulco to 4.4 m s^{-1} (370 km day^{-1}) near Guaymas. They also call attention to the existence of solitary, energetic events of elevation that occur only during the summer–fall season, and whose alongshore coherence and propagation are evident from time series plots. Based on estimates of phase speed, volume

transport and offshore scale, they conclude that the fluctuations are most consistent with internal Kelvin waves, while probably being of a more general (hybrid) type in which topographic effects are important.

In this paper we focus on several aspects of the variability off Mexico that are complementary to the study of Christensen *et al.* (1983): 1) examination of individual, large amplitude events; 2) documentation of how the propagating variability is generated; 3) frequency domain analysis of the sea level fluctuations; and 4) consideration of the seasonality of the propagating variability and its forcing.

Following a summary of the data used (Section 2), the occurrence of tropical storms and their relation to individual sea level events are discussed (Section 3) and the statistical evidence for forcing is presented (Section 4). The observed characteristics of alongshore propagation are then examined through spectral analytical techniques (Section 5) and compared with those expected from theory (Section 6).

2. Data

Table 1 lists information pertinent to the primary data set used in this investigation, which consists of six-hourly time series of sea level height (SLH), sea level atmospheric pressure (SLP) and surface winds, at or near seven stations from San Jose, Guatemala (13°N) to Guaymas, Mexico (28°N) (shown in Fig. 1). The SLH data covers two periods: May–December 1971 and January 1973 through December 1975. The 1971 SLH data are used primarily to increase the information available for our analysis of individual, large-amplitude events, while most of the statistical results are based on the longer 1973–75 time series.

The sea level heights were derived from hourly tide data obtained from the Inter-American Geodetic Survey, Guatemala (San Jose only) and the Centro de Investigacion Cientifica y Enseñanza Superior de Ensenada (CICESE; all other stations). The hourly data was carefully processed to eliminate erroneous tabulations and datum jumps. Short gaps were bridged by adding predicted tides to the linearly interpolated anomalies from the predicted tides. Six-hourly time series of SLH were then computed by low-pass filtering the hourly data, using a cosine–Lanczos filter with a half power point at 0.60 cpd (40 hours).

The SLP data for 1973–75 were interpolated to the station locations from six-hourly gridded analyses produced by the Fleet Numerical Oceanography Center (FNOC, Monterey). The quality of the SLP data from FNOC was verified by correlation with reported pressures from coastal airports, when the latter were available (the correlation coefficients are listed in Table 1).

The subsurface pressures (adjusted SLH) were obtained for the 1973–75 data by adding the FNOC pressures (minus 1000 mb) to the filtered (unadjusted) SLH data. Final SLH time series were obtained by regressing on neighboring stations (not used in the investigation) to fill four gaps of less than a month, and by removing the three-year annual harmonics (the harmonic coefficients are listed in Table 1). All of the 1973–75 time series of SLH were complete (i.e., 36 months), except for Topolobampo and Mazatlan, which begin at the same time as the others but end after 24 and 30 months, respectively. The sea level heights for 1971 were processed as described above, except that they were not adjusted (for lack of atmospheric pressure data) and the annual harmonics removed were those computed for 1973–75 (Table 1).

Wind data for 1973–75 were derived from log sheets of synoptic weather observations, obtained through CICESE, for Mexican airports at Guaymas, Mazatlan, Acapulco and Salina Cruz. Tabulation errors were corrected, inconsistencies in units were eliminated, and nocturnal gaps were bridged by a three-point Lagrangian interpolation to six-hourly intervals. The six-hourly winds were then low-pass filtered in the same way as SLH. Large gaps remained, which are listed in Table 1.

3. Storm forcing of energetic events

a. 1971

Fig. 2 shows the time series of coastal sea level for the period 1 May to 31 December 1971. The plotted

TABLE 1. List of stations, symbols, locations, and relevant information regarding the data, including: the average correlation for successive four month periods, between the observed and FNOC atmospheric pressures (r_p); the three-year (1973–75) standard deviation of adjusted sea level heights, with their annual cycle removed ($\langle \zeta' \rangle$); and the harmonic amplitude (a_{12}) and phase (θ_{12}) of the annual cycle of sea level.

Station	Symbols	Latitude	Longitude	r_p	$\langle \zeta' \rangle$ (cm)	a_{12} (cm)	θ_{12} (deg)	Gaps in wind record
Guaymas	GU	27.9	110.9	0.821	6.37	15.4	215	2/1/73–7/31/73; 10/1/73–10/31/73
Topolobampo	TO	25.6	109.1	—	6.93	14.1	221	No wind data acquired
Mazatlan	MZ	23.2	106.4	0.804	7.49	8.0	229	Data could not be used
Manzanillo	MN	19.1	104.3	0.819	6.99	6.4	230	No wind data acquired
Acapulco	AC	16.8	99.9	0.718	6.86	5.8	228	6/1/74–6/20/74; 12/19/74–1/21/75
Salina Cruz	SZ	16.2	95.2	0.802	7.94	7.0	192	7/29/75–9/5/75
San Jose	JO	13.9	90.8	—	7.78	3.4	230	No wind data acquired

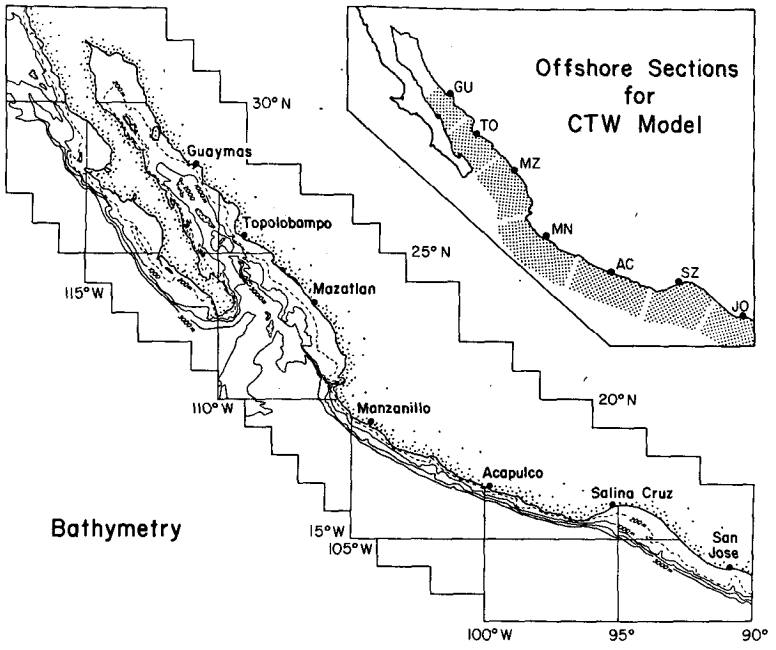

FIG. 1. Locations of sea level stations and bathymetry chart for the Pacific coast of Mexico, with isobaths shown for depths of 200 m (dashed) and 1000, 2000 and 3000 m (solid). Inset at upper right is a map showing the coastal sections for which the coastal-trapped wave model of Brink (1982) was run (Section 6).

series have been demeaned and the plots are separated in proportion to the distance between stations. The series clearly show part of the annual cycle, with generally higher July–September sea level in the north associated with the greater upper ocean heat content found in the Gulf during summer months (Roden, 1964). Superimposed on the annual increase, and occurring in random sequence, are solitary, large-amplitude events of elevation. These events are especially prominent from Acapulco northwestward, highly coherent, and have a clear phase propagation. It was pointed out by Christensen *et al.* (1983) that these events characteristically occur during summer months.

Our first concern was to locate a likely generating mechanism for these energetic events. Eastern North Pacific (ENP) tropical cyclones could explain a number of features found in the data. The ENP tropical cyclones that reach "tropical storm" intensity occur almost exclusively during the five month warm season from mid-May through mid-October, with a locus of maximum occurrence that parallels the Mexican coast about 300 km offshore, from Salina Cruz to Manzanillo (Thompson and Ellsberry, 1981; see Fig. 3). From the statistical distribution of storm centers, one expects Salina Cruz to be affected less often than stations immediately to the northwest. Moreover, since the storm centers are found almost always at sea, and not over land, the storm winds most likely to occur in the coastal region would be southeasterly and would thus favor the generation of sea level rises,

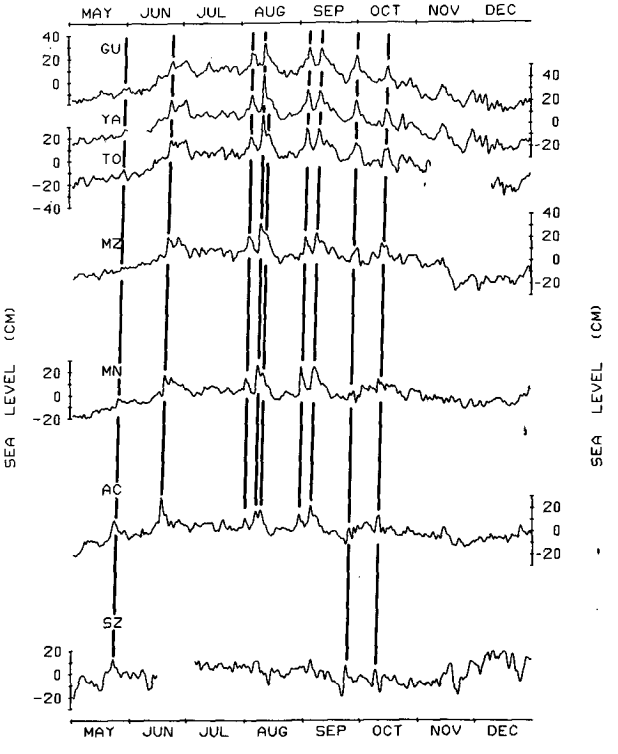

FIG. 2. Low-pass filtered sea level heights at tide stations on the mainland coast of Mexico, in 1971 (annual harmonic not removed). Time series are vertically spaced in proportion to the station separations. Location abbreviations are defined in Table 1, except YA (Yavaros, 27°N). Straight lines indicate propagating events associated with tropical storms.

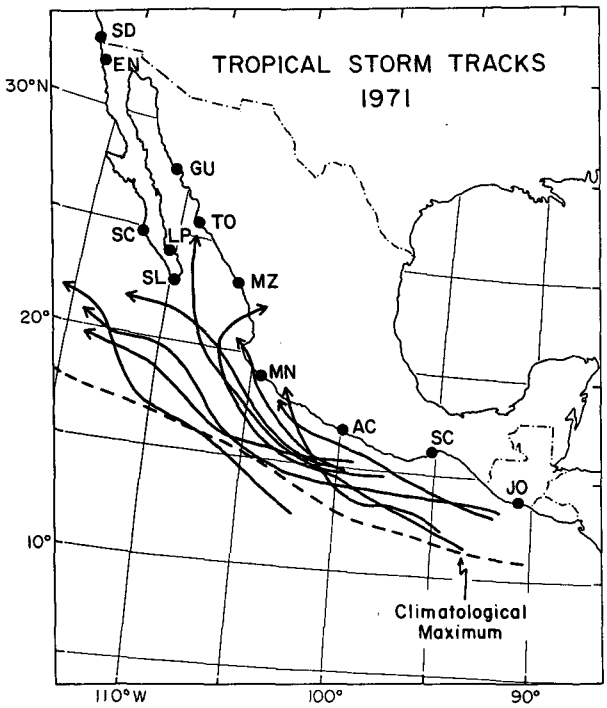

FIG. 3. Tracks of tropical storm centers that passed within 500 km of the Mexican coast in 1971 (solid lines). Dashed line indicates the locus of maximum occurrence of tropical storm centers (Thompson, *et al.*, 1981).

rather than falls. Finally, since by definition the classifications "tropical storm" and "hurricane" imply maximum sustained winds of at least 17 m s^{-1} and 28 m s^{-1}, respectively, the sea level events produced by such storms would be of large amplitude, appearing as solitary occurrences.

Fig. 3 shows the tracks of the centers of all cyclones that reached tropical storm intensity in 1971, and passed within 500 km of the mainland coast (redrawn from Denney, 1972). Due to the wind distribution typically found around tropical storms (Rhiel, 1954), it is unlikely that storms found farther offshore than 500 km could produce large-amplitude responses in coastal sea level. There was much ENP storm activity in 1971, with 18 tropical storms reported by the Eastern Pacific Hurricane Center (EPHC, Redwood City, California), of which 12 reached hurricane intensity. Of the 18 storms, nine were close enough to the mainland to affect coastal sea level, seven of them being hurricanes (Fig. 3). Some descriptive data on these nine storms is listed in Table 2. In every case, a sea level event of elevation was found at Acapulco, near the time of storm occurrence there, that subsequently propagated northwestward to Guaymas. These propagating events are highlighted by straight lines in Fig. 2. The remaining nine storms tracked more than 500 km offshore and were not associated with coastal sea level disturbances.

Eastern North Pacific tropical storms develop from immature cyclones that form out of disorganized squall activity, usually off Guatemala or the Gulf of Tehuantepec. Crutcher and Quayle (1974) show climatological charts of the movement of ENP tropical storm centers. Cyclones are typically found within 500 km of Salina Cruz or Acapulco when they are officially recognized as tropical storms by the EPHC. They then develop to their maximum intensity while moving either to the northwest (NW) or west-northwest (WNW), often becoming hurricanes. Whichever direction they move in, storms beginning at Salina Cruz can affect the coastal area locally and also at Acapulco. Storms beginning off Acapulco, however, are less likely to have affected the Gulf of Tehuantepec (Salina Cruz). This helps explain why the propagating sea level events (Fig. 2) are less often recognized at Salina Cruz, and why sea level correlations involving Salina Cruz are lower (Christensen *et al.*, 1983). If a storm travels NW from Acapulco, it is likely to remain close enough to the coast to influence coastal sea level at least to Manzanillo, whereas if it moves WNW, its influence may cease to be felt much beyond Acapulco. Either way, climatology shows that

TABLE 2. Names, dates, speeds of, and stations affected by near-coastal tropical storms reported by the Eastern Pacific Hurricane Center (EPHC) for 1971. Also shown are the maximum winds reported at Acapulco (AC), Salina Cruz (SZ), Mazatlan (MZ) and Guaymas (GU) during the three-day period leading up to and including the sea level event passage at each station. An asterisk indicates that a storm reached hurricane intensity. Wind speeds in boldface are greater than the mean plus one standard deviation (see text).

EPHC number	Name	Month/Day	Storm speed (km day^{-1})	Stations affected	Maximum wind (m s^{-1})			
					SZ	AC	MZ	GU
1	*Agatha	5/21–5/24	370	SZ–MN	6.0	**10.0**	4.0	3.1
2	*Bridget	6/14–6/20	500	SZ–AC	6.0	**42.5**	3.0	4.1
9	*Ilsa	7/30–8/8	620	AC–MN	6.0	**13.0**	3.1	3.0
10	Jewel	8/6–8/11	350	AC–MN	7.3	**18.0**	3.6	3.8
11	Katrina	8/8–8/12	410	SZ–MN	7.3	**8.0**	3.1	3.8
12	*Lily	8/28–8/31	360	SZ–MN	**12.0**	**7.5**	**8.0**	5.3
14	*Nanette	9/2–9/9	370	AC–MN	**8.0**	**14.8**	4.0	5.0
15	*Olivia	9/20–9/30	490	JO–MN	**12.0**	**10.0**	2.0	3.8
16	*Priscilla	10/6–10/1	430	SZ–MN	**10.7**	**11.0**	2.5	4.4

the storm centers most frequently turn westward before reaching 20°N. Occasionally, in September or October, tropical storms and hurricanes move northward into the Gulf of California, after first leaving the near-coastal area farther south. By the time they return to the coastal area they are in a dissipating stage, but often cause damage between Mazatlan and Guaymas (Roden, 1964). Compared to storms that leave the coastal region south of 20°N (never returning), storms that affect the Gulf of California are rare.

To further document the association between tropical storms and coastal sea level events, we examined time series of the maximum daily winds reported at coastal airports at Salina Cruz, Acapulco, Mazatlan and Guaymas. The maximum winds reported during the three-day period ending just after the sea level event passage at each station are also shown in Table 2. As a reference for comparison, the mean and standard deviation of maximum daily winds at Acapulco for August–October, in a three year period (1973–75) were 4.6 and 2.8 m s^{-1}, respectively. The wind statistics for the same months are very similar for Salina Cruz and Mazatlan, but somewhat smaller for Guaymas. In all cases the winds at Acapulco appear unusually strong during the periods of storm/event occurrence, but less frequently so at Salina Cruz. The winds at Mazatlan and Guaymas did not reach unusual intensities any more frequently than would be expected by chance. Hence, both the cyclone tracks and the reported coastal winds indicate that propagating sea level events are typically forced by tropical storms along the southern Mexican coast, and continue poleward as free waves northwest of Manzanillo.

The atmospheric pressure observations for Salina Cruz, Acapulco, Manzanillo, Mazatlan and Guaymas were examined to see if unusually low pressures occurred during the sea level event passages. Such low pressures are found within ~100 kilometers of tropical storm centers, and could conceivably explain the large elevations found in the 1971 unadjusted sea level records (Fig. 2). Abnormal pressures could not be found, however, even when large wind speeds were reported.

To further explore the likelihood of forced propagation in the south versus free propagation in the north, we determined the propagation speeds of the nine storm-related events (Fig. 2) for station pairs with separations of up to 1100 km. This was done by dividing the distance between stations by the corresponding travel time of the event (at maximum sea level). The propagation speeds for these events are summarized in Table 3. Much of the scatter is due to uncertainties in the determination of travel times. A travel time difference of one data interval implies speed differences of up to 120 km day^{-1}, depending on station separation. The mean speeds decrease poleward, and the scatter in speeds poleward of Manzanillo is systematically less than farther south. The higher event propagation speeds in the southern region compare favorably with the observed storm speeds (Table 2), while the event speeds farther north are more in agreement with those of free hybrid coastal-trapped waves supported by stratification and topography (see Section 6). The large scatter in speeds at southern stations cannot be adequately explained by the uncertainties in estimation, but are reasonable under the assumption of alongshore forcing by the storms, which show a wide range of travel speeds (Table 2). The lower scatter in speeds at the northern stations is within the uncertainty of estimation, consistent with free coastal trapped waves, whose speed would only vary in time in proportion to stratification changes.

TABLE 3. Statistical summary of propagation speeds from the event analysis of storm-related sea level disturbances in 1971.

Station pair	Separation (km)	Propagation speed (km day^{-1}) Mean	Standard deviation	Minimum	Maximum	Range
GU–TO	320	229	100	107	427	320
GU–MZ	670	220	29	168	255	87
TO–MZ	360	283	70	206	360	154
TO–MN	920	299	71	238	460	222
MZ–MN	560	274	43	204	344	140
MZ–AC	1090	322	83	242	484	202
MN–AC	530	351	163	223	707	484
MN–SZ	1080	462	159	332	720	388
AC–SZ	550	498	164	314	733	419

b. 1973–75

To determine if the results of the 1971 event analysis could be corroborated for other years, we repeated the event analysis for the 1973–75 data set. The three-year time series, with their annual harmonics removed, are shown in Fig. 4 for stations from San Jose to Guaymas. The large-amplitude events of elevation are limited to the summer tropical storm period, while at Salina Cruz there are energetic events of depression during winter months. The latter are evidently associated with strong northerly winds blowing across the isthmus from the Caribbean to the Gulf of Tehuantepec (Section 4). Unlike the summer events, the winter events do not appear to propagate poleward.

The summer association between large-amplitude propagating sea level events and tropical storm activity off southern Mexico is also a feature of the 1973–75 data, with forcing limited to the south and propagation speeds decreasing northwestward. The most notable difference from 1971 is the reduced frequency of occurrence (about half) of both the large-amplitude events and the associated near-coastal

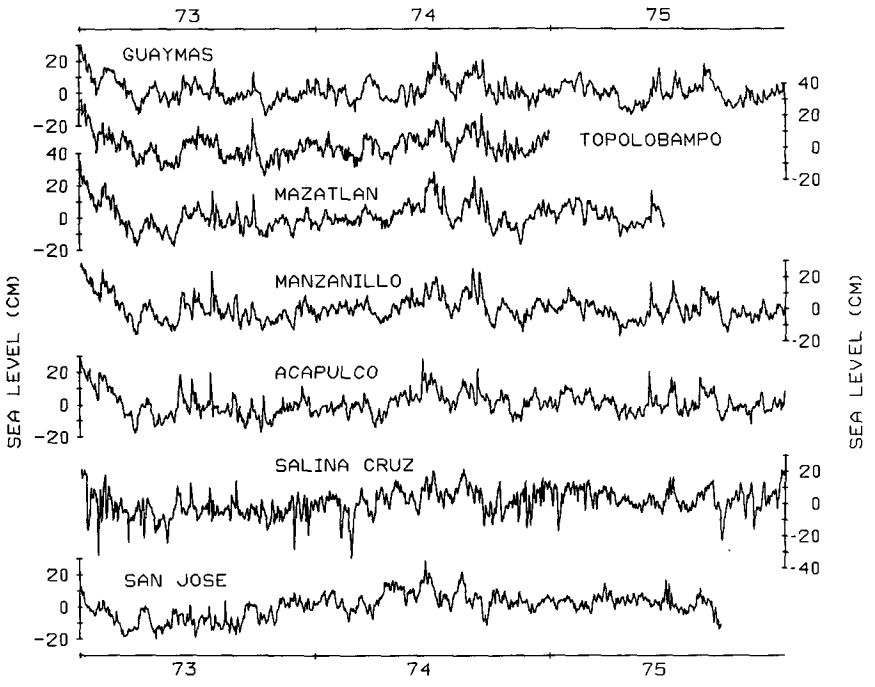

FIG. 4. Low-pass filtered sea level heights (annual harmonics removed) for the coast of Mexico and Guatemala in 1973–75. Time series are vertically spaced in proportion to the station separations.

tropical storms. This is consistent with the fact that 1971 was an exceptionally active year for ENP tropical storms (18), while the 1973–75 period averaged about nine tropical storms per year (Gunther, 1980).

Fig. 5 shows two case histories that are illustrative of the storm/event associations. At Acapulco, hurricanes "Emily" (July 1973) and "Norma" (September 1974) were both associated with winds of 15–20 m s^{-1} lasting for at least 24 hours prior to and during the culmination of rapid sea level rises (about 20 cm in 36 hours). Emily began in an area of squalls in the Gulf of Tehuantepec (off Salina Cruz), developing to hurricane force just south of Acapulco. She then moved west-northwest at 500 km day^{-1} along a track nearly parallel to the coast and 300 km offshore, occasioning ship reports of gale-force winds off the coast just northwest of Acapulco (Baum, 1974). The sea level event raised by Emily traveled from Salina Cruz to Manzanillo at a speed of 400 km day^{-1}, and increased in magnitude. Norma, unlike Emily, began southwest of Acapulco and moved directly onshore, causing three deaths from mudslides (Baum, 1975). The sea level event raised by Norma traveled from Acapulco to Manzanillo at a speed of only 220 km day^{-1} and did not increase in amplitude. There is no ready explanation for the lack of a sea level maximum at Topolobampo following hurricane Emily, other than the fact that the Topolobampo tide gauge is located in an area of complex coastline with islands and inlets, where local variations may sometimes obscure larger scale variability.

In summary, case history analysis of four years of data shows that large-amplitude propagating events of elevation along the Pacific mainland coast of Mexico, characteristic of summer sea level records, are generated by near-coastal tropical storms off southern Mexico. Coastal wind records, event-related storm tracks and storm climatology all indicate that the forcing occurs along the stretch of coast from Salina Cruz to Manzanillo. At stations in the southern forcing region, propagation speeds have large means (350–500 km day^{-1}) and standard deviations (>150 km day^{-1}), apparently dependent on the large and variable storm speeds. North of Manzanillo, the storms cease to accompany the events they generate. There the event speeds decrease to the range of 220–320 km day^{-1} (average) and tend to be more time-invariant (standard deviations $\leq$ 80 km day^{-1}). Other, smaller events can be seen in the records that may also propagate, but for which we cannot identify specific causes. Many smaller storms ("chubascos") are known to occur seasonally along the Mexican coast (Roden, 1964), which escape the notice of the weather services and may play a role in forcing the less energetic variability.

4. Statistical analysis of sea level forcing

In general, one can hypothesize that the sea level variability at a particular tide station is the product of local, large scale and remote processes. We have data for three parameters that may be representative

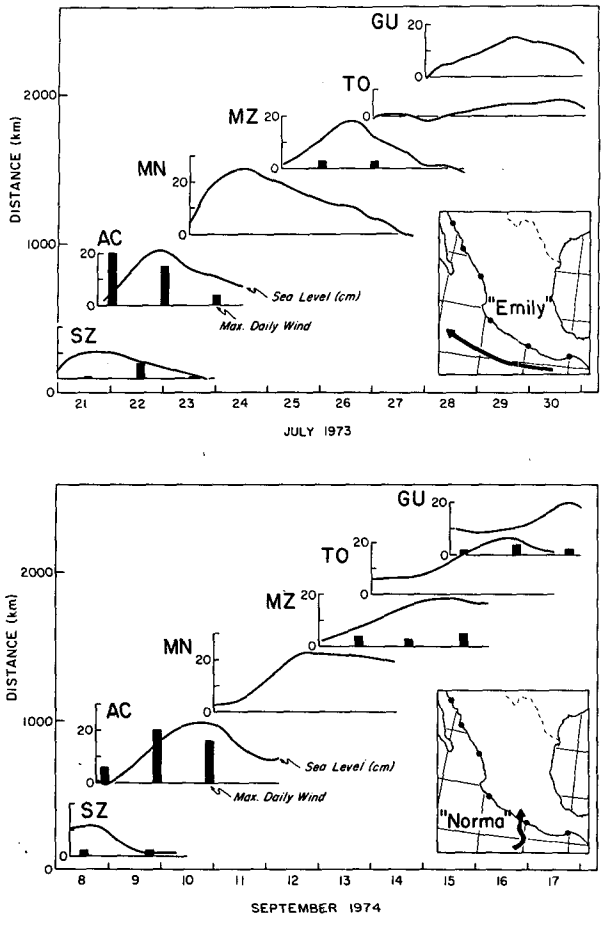

FIG. 5. Case history diagrams for two propagating sea level events. A time-distance plot of sea level height (solid line, cm) and maximum daily winds (vertical bars, m s^{-1}) during the passage of an event is shown for each tide station, with its origin at the appropriate time and position. The inset maps show the hurricane tracks associated with the sea level events. No wind observations are available for the stations at which wind bars are not plotted.

of such processes: winds, atmospheric pressure and sea level itself. In this section we first examine the separate effects of wind and pressure, and then—through multiple regression—the combined effects of all postulated factors.

In our analysis, we analyzed seasonal segments of the greatest length possible taken from the three-year (1973–75) data set for the three stations at which we had sufficient information on sea level, winds and pressure: Guaymas, Acapulco and Salina Cruz. We defined five 150-day periods: the three summers (mid-May through mid-October)[1] of 1973, 1974 and 1975 and the two intervening winters (mid-November through mid-April). Due to large gaps in the wind data, four station/seasons could not be analyzed: Guaymas/summer 1973, Guaymas and Acapulco/winter 1974–75, and Salina Cruz/summer 1975. For simplicity and clarity, we will often show only results for the two complete seasons (winter 1973–74, summer 1974). The important results for these seasons are corroborated by those for the other periods.

a. *Wind effects*

For each of the three stations, wind components were computed in the direction of dominant forcing, that is, in the direction for which the wind component produces the largest response (Garrett and Toulany, 1982; see Appendix A). It was found that winds from the southeast, east and south are most efficient at raising sea level at Guaymas, Acapulco and Salina Cruz, respectively. All future references to wind variability are based on analyses using wind components from these directions.

The local effects of wind were examined by computing the correlations between sea level and the local wind at each station for each of the five seasonal time segments. In the following discussion, the correlation magnitudes appear in chronological order where significant at the 95% level of confidence, or are indicated as "ID" where insufficient wind data existed. A contrasting seasonal behavior was found for Guaymas and Acapulco, as opposed to Salina Cruz: The summer correlations, are moderate to strong at Acapulco (0.52, 0.40, 0.38) and Guaymas (ID, 0.37, 0.41), and insignificant at Salina Cruz. Winter correlations are strong at Salina Cruz (0.54, 0.66), but insignificant at Guaymas and Acapulco.

The coherence spectra between sea level and local wind are shown in Fig. 6 for station/seasons with high wind–SLH correlations. During the summer months, Acapulco shows significant, broad-band coherence over the 0.05–0.33 cpd frequency range. At Guaymas there is low to marginal (95% significant) coherence over the same range. At higher frequencies, corresponding to periodicities of 3 days or less, wind and sea level are incoherent at both stations. The phase spectra (not shown) indicate that sea level at these stations responds to wind forcing after a delay of 1–2 days. In winter, periods of strong northerly winds occur at Salina Cruz, where cross-spectra between sea level and winds show relatively high coherence in two ranges, 0.05–0.26 cpd and 0.37–0.51 cpd, separated by an incoherent band (0.26–0.37 cpd). The highest coherence at Salina Cruz occurs in the very-low-frequency band corresponding to periodicities of 6 to 20 days. It is this latter range that corresponds to the series of energetic negative events in winter sea level at Salina Cruz, visible in the plotted time series (Fig. 4). The phase spectrum indicates that a sea level decrease in response to northerly wind forcing is almost immediate (perhaps a few hours, which the data cannot resolve).

Remote effects can be seen in the correlations between sea level at one place and winds at remote

[1] Due to a data gap, the 1974 summer period begins in mid-June and ends in mid-November.

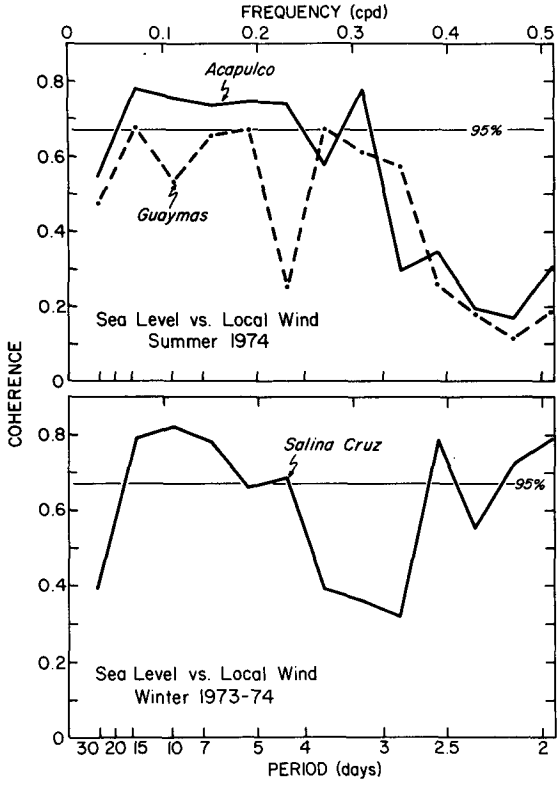

FIG. 6. Coherence spectra between sea level and local wind for the three cases in which the multiple-input forcing model showed a significant contribution from the local wind (Table 5). The 95% significance level is indicated.

locations. Fig. 7 shows the maximum lagged correlations (summer, 1974) between the winds at Acapulco and Guaymas, and sea level at each of the seven mainland stations. The Acapulco wind is a significant source of variability for summer sea level at stations as far away as Guaymas. In fact, the sea level at Guaymas is about as well correlated with the Acapulco wind as with the local wind, even though the winds at the two locations are poorly correlated with each other. Also, sea levels lag the Acapulco wind in a way consistent with the observed poleward sea level event propagation. In contrast, the Guaymas wind loses its correlation very quickly with stations equatorward of Guaymas. These results are consistent with those of the event analysis, which show that the summer winds generate poleward propagating sea level events in the region of Acapulco. It is clear that the wave propagation process is transmitting considerable information poleward through the coastal waveguide.

b. *Pressure effects*

As noted in Section 2, the sea level time series have been adjusted for the effect of atmospheric pressure. This does not preclude the existence of a residual correlation between sea level atmospheric pressure (SLP) and the adjusted sea level height (SLH), which may come about, e.g., from the correlation between pressure and some third variable that forces sea level, such as local wind or large scale synoptic weather patterns. Examples of this may be seen in the analysis of Chelton and Davis (1982).

Maximum lagged correlations were computed between SLH and SLP for the various station/seasons. The SLP is usually marginally correlated with SLH near the 95% level of confidence, and explains less than 10% of the SLH variance. Also, the local wind correlates more highly with both SLH and SLP than does SLP with SLH. Thus, a small residual correlation does occur, but part of it is probably due to the correlation between SLP and local wind. Two exceptions to the pattern of marginal correlations are worth mentioning. First, the SLH–SLP correlations at Acapulco were never significant in summer (even at the 80% confidence level). Second, the SLH–SLP correlations were relatively high at Acapulco and Salina Cruz in winter, especially the winter of 1973–74.

The most significant aspect of the atmospheric pressure is its large-scale character. An empirical orthogonal function (EOF) analysis of SLP was done for the seven stations from Guaymas to San Jose. The first EOF, which we shall refer to as the SLP mode, explained 84% of the total SLP variance for the 1974 summer and 75% for the 1973–74 winter. As expected, the SLP mode and local SLP are very similarly correlated with SLH. Table 4 shows the intercomparison of local SLP, local wind and the SLP mode at the seven stations, for the 1974 summer and the 1973–74 winter. The largest correlations are for local SLP with the SLP mode. In fact, they are so large as to suggest that local SLP variability is largely a reflection of large scale atmospheric processes. Finally, we note from the correlations between winds and the SLP mode that some 30–45% of the wind variance at Salina Cruz is coupled to the large scale pressure

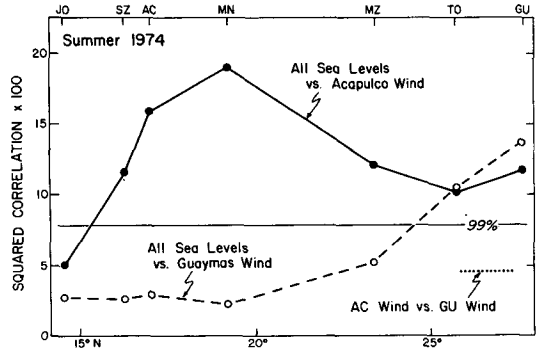

FIG. 7. Squared maximum lagged correlation (×100) between the Acapulco wind and sea level everywhere (solid), the Guaymas wind and sea level everywhere (dashed), and between the two winds (dotted), for the summer of 1974. The 99% significance level is also shown.

TABLE 4. Correlation coefficients, for selected summer and winter seasons, between sea level pressure (SLP), winds and the first mode (EOF) of sea level pressure. Values shown in boldface are significant at the 99% confidence level or better.

	Summer 1974			Winter 1973–74		
Station	SLP mode versus local SLP	SLP mode versus local wind	Local SLP versus local wind	SLP mode versus local SLP	SLP mode versus local wind	Local SLP versus local wind
GU	**0.94**	**−0.26**	**−0.36**	**0.77**	**−0.24**	**−0.31**
TO	**0.96**	—	—	**0.86**	—	—
MZ	**0.97**	—	—	**0.93**	—	—
MN	**0.92**	—	—	**0.91**	—	—
AC	**0.89**	0.24	0.23	**0.91**	0.16	0.14
SZ	**0.83**	**−0.55**	**−0.57**	**0.88**	**−0.66**	**−0.86**
JO	**0.70**	—	—	**0.85**	—	—

fluctuations as represented by the first SLP mode. Such coupling is much weaker at Acapulco and Guaymas, accounting for less than 7% of the variance.

c. *A multiple input forcing model*

For the purpose of analyzing the combined effects of possible forcing parameters, we examine three ways in which sea level at a given location on the Pacific mainland coast of Mexico may be influenced: 1) by wave propagation from a remote source of forcing to the southeast; 2) by coastal wind forcing; and 3) by large scale atmospheric processes, which may in turn force and therefore represent large scale oceanic motions. Some of the variables that can be used to represent these influences are, in general, correlated with each other, so that simple bivariate analysis between sea level and other variables can be misleading (Chelton and Davis, 1982). Multiple regression of sea level on assumed forcing variables is a preferable approach, because each partial regression coefficient is determined only by the part of the corresponding input variable that is uncorrelated with other inputs (Snedecor and Cochran, 1980; section 17.5). We therefore formulated a multiple input forcing model to describe the response of sea level at Guaymas, Acapulco and Salina Cruz to the above influences.

Sea level at southern stations is used to represent wave propagation in the model (Acapulco for Guaymas, Salina Cruz for Acapulco and San Jose for Salina Cruz). Local winds are used to represent coastal wind forcing at each station, and the SLP mode to represent the large scale atmospheric influence on sea level. The wind at a remote location is included to insure that remote processes are adequately represented (the Acapulco wind was used for Guaymas, Salina Cruz for Acapulco, and Acapulco for Salina Cruz). We note, however (from Fig. 7), that a contribution from remote winds may represent a distant source of wave-propagated variability, as well as remote atmospheric activity. Each input variable was optimally lagged with respect to the response variable in agreement with the maximum lagged correlation between them.

The results from the four-input forcing model are given in Table 5. As a measure of the relative importance of the j-th input to the modeled response, we have tabulated the statistic 100 R_j^2, where $R_j = b_j(S_j/S_y)$, b_j is the regression coefficient for the j-th input, and S_j, S_y are the standard deviations of the j-th input and the estimand (SLH), respectively. In statistical terminology (e.g., Snedecor and Cochran, 1980), the R_j's are the standard regression coefficients, i.e., the regression coefficients scaled to account for the natural variabilities of the inputs. When the inputs are independent (i.e., their intercorrelations are zero), the statistic R_j^2 is the sample estimate of the fraction of variance in the estimand attributable to its linear regression on the j-th input. In general cases R_j^2 can be used as a measure of the relative importance of the input variables to the overall model, with the understanding that if the intercor-

TABLE 5. Results of a multiple-input forcing model for sea level at Guaymas (GU), Acapulco (AC) and Salina Cruz (SZ). The first four double-entry rows are for the input (forcing) functions, and the last row is for the total model output. The top values in the input rows are a measure of the relative importance of the inputs to the model output ($100R_j^2$, as defined in the text). The bottom values are the percent variance explained by each input, based on the lagged correlation between sea level and that input (single-input regression). The last row gives the percent variance in the estimand (sea level) explained by the model output. Values in boldface are significant at the 99% confidence level.

	Winter 1973–74			Summer 1974		
	GU	AC	SZ	GU	AC	SZ
Remote sea level	2.6	0.3	**17.0**	**37.3**	**27.2**	**42.0**
	5.8	2.4	**23.1**	**32.8**	**36.0**	**48.9**
Local wind	4.0	0.2	**40.3**	**8.2**	**9.2**	0.5
	4.6	3.1	**29.5**	**13.7**	**15.9**	7.8
Remote wind	0.1	4.6	2.0	**7.8**	2.8	0.9
	1.6	**9.4**	3.9	**12.3**	10.2	7.6
Pressure mode	3.9	**8.1**	1.6	0.8	0.2	1.0
	6.5	**18.8**	**22.3**	7.4	7.3	6.0
Model response	12.3	**21.0**	**56.1**	**68.3**	**49.1**	**51.9**

relations are high, it may not be possible to correctly disentangle the effects of the inputs. For comparison with the results obtained from bivariate analysis (single-input regression), the percent sea-level variance explained individually by the optimally lagged inputs is also shown. The last row in Table 5 gives the square of the multiple correlation coefficient multiplied by 100, or the percent variance in sea level explained by the four-input model.

An advantage of optimally lagging the inputs with respect to the estimand (sea level) is that the input variables are seldom lagged optimally with respect to each other, generally making the intercorrelations small. Thus, for example, the Guaymas regressions involved large lags between SLH at Guaymas and the remote inputs of sea level (7 days preceding) and wind (5½ days preceding) at Acapulco. This has the effect of making the latter two variables virtually independent of each other at the resulting lag (wind lagging local sea level by 1½ days). In fact, there were *no* appreciable intercorrelations in either the summer or winter regressions for Guaymas, making interpretation of the results straightforward. For the Acapulco and Salina Cruz regressions, the remote inputs were geographically closer and have smaller lags that permit larger intercorrelations. However, only a total of five intercorrelations were appreciable, e.g., greater than 0.35: the four occurrences of Salina Cruz wind versus the SLP mode (0.52–0.64), plus the Salina Cruz wind and sea level (0.41) during summer, which were used as remote inputs for Acapulco.

Sometimes the effect of intercorrelations is clear. For example, based on single-input models, both the local wind and the SLP mode appear important to Salina Cruz sea level in winter, with the wind better correlated. But in the four-input model the SLP mode is unimportant due to its high intercorrelation with the Salina Cruz wind (0.64). Not all entries in Table 5 are as easily understood, however. The greater the number of intercorrelations that exist the more obscure will their effect be, because the contribution of a particular term in an M-input model will depend on its multiple regression on the other M-1 inputs.

The model shows that a remote transfer of sea level variability, through propagation, is the most important process during the summer. Local winds provide some additional forcing at Guaymas and Acapulco, while remote winds are only important at Guaymas (consistent with Fig. 7). In winter, the model only performs well at Salina Cruz, where the local wind is the dominant influence, and covariability with sea level just equatorward (San Jose) is of secondary importance. Note, however, that the effect of the winter wind on sea level at Salina Cruz, while considerable, is not transmitted poleward to Acapulco and Guaymas through wave propagation. This confirms statistically what can be seen in Fig. 4. Finally, the SLP mode did not emerge as an important source of forcing, in general, though it does contribute to the winter sea level variability at Acapulco.

5. Sea level coherence and propagation

As an overall measure of sea level coherence and propagation over a wide range of frequencies, we computed the maximum lagged crosscorrelations between stations and the propagation speeds implied by their lags. These results are described in Appendix B and discussed at the end of this section. We have found, however, that frequency domain analysis is the preferable way to analyze for propagation effects, because incoherent bands can be excluded from consideration (or assigned a lower weighting), whereas their presence in correlation statistics may, in general, introduce bias into the estimates of phase propagation. Thus, for example, Enfield and Allen (1980) found a large-scale, poleward propagation in monthly sea level anomalies along the eastern Pacific boundary, but the overall speed determined from lagged correlations (180 km day^{-1}) was much larger than that found from cross-spectral analysis (75 km day^{-1}). The former included large contributions of incoherent energy at high frequencies, while the latter considered only the low-frequency, coherent bands.

a. Autospectra

The time series for summers (but not winters) are characterized by isolated, energetic events of elevation separated from each other by unequal time intervals (e.g., Fig. 2). A time series of identical Gaussian bumps, spaced equally in time at intervals Δt, Fourier transforms to a spectrum with successively smaller, multiple peaks centered at frequencies f_0, $2f_0$, $3f_0$, etc., where $f_0 = (\Delta t)^{-1}$. If the spacing between bumps is non-uniform the spectral signature becomes blurred and the peaks may be difficult to resolve from the background energy level. This is especially true at higher frequencies where the peaks are smaller.

In computing the autospectra we sought to optimize the resolution by analyzing eight-month time series segments centered on summer and winter seasons, with band averaging to achieve a bandwidth of 0.02 cycles per day (cpd) and 10 degrees of freedom (df) per band. Because peaks are certain to occur, not all of them significant nor necessarily related to a common process amongst stations, the autospectra for all stations from Acapulco to Guaymas were averaged together for a given season. Examples are shown in Fig. 8 for the 1974 summer and the 1973–74 winter. The features of Fig. 8 are also representative of other years. The confidence limits are a function of frequency due to the dependence of the degrees of freedom on the coherence between stations. The limits are largest for perfect coherence (10 df) and smallest for null coherence (50 df); both extremes

are shown in Fig. 8, for the 90% level of confidence. Note that the true confidence limits (unknown) will be smaller at the higher frequencies, where the coherence between stations is lower (see the discussion of coherence, below).

The autospectra of sea level are red, with a typical rolloff of two decades over the 0–0.25 cpd frequency range. There is a consistent tendency for multiple peaks to occur in the summer spectra. In 1971 an energy maximum usually occurs in the 0.09–0.17 cpd range, while in 1973 and 1974 the more common range is 0.06–0.10 cpd. Other maxima occur more erratically at higher frequencies, e.g., 0.27–0.35 cpd in 1971 and 0.16–0.24 cpd in 1974. The winter autospectra have generally similar energy levels to those of summer. However, the winter spectra lack a multiple-peak structure that is consistent from one station to another, as in summer. We think the multiple peaks in summer autospectra are related to the large-amplitude propagating events, first, because both the events and the multiple spectral peaks occur in summer but not in winter, and second, because the summer energy peaks tend to occur at harmonic frequencies in a way that is consistent with time series dominated by energetic events of elevation. The observed spectra then imply average time intervals between energetic events of about 8 days in 1971 and 12 days in 1973–75, which appear reasonable.

b. *Characteristics of coherence spectra*

The cross spectra of sea level were computed from the five-month seasonal data segments, with band averaging to achieve a bandwidth of 0.04 cpd and 12 df per band. An example of the spectra from the 1971 summer data is shown in Fig. 9.

The sea level coherence is typically highest, and most often significant, at the lowest frequencies. In the summer of 1971, significantly high coherence exists over a relatively wide range of frequencies (Fig. 9). There is a more rapid decay of coherence with increasing station separation in the band centered at 0.07 cpd (two weeks), while the coherence remains strong over large distances in the band centered at 0.11 cpd (nine days). The latter band corresponds to the low frequency power peak already noted. The upper panel of Fig. 10 shows the relative frequency of occurrence of coherences, significant at the 90% confidence level (0.6) for summers and winters. Summer coherences in the 0.02–0.21 cpd range are significant about twice as often as in winters, and several times more often than at higher frequencies.

To understand the alongshore structure of sea level coherence, we ensemble-averaged the 1973–75 cross spectra by season for neighboring stations, then frequency-averaged over the three lowest frequency bands spanning the range 0.02–0.13 cpd.[2] This range corresponds to periodicities of 7–50 days, at which both the autospectral energies and the alongshore

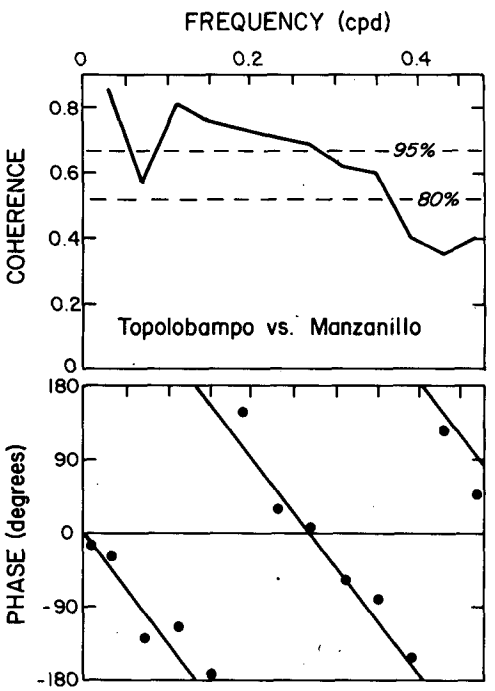

FIG. 9. Coherence and phase spectra between Topolobampo and Manzanillo. Phase values (dots) indicate that the southern station leads. Phase line is a weighted regression fit (see Section 5c).

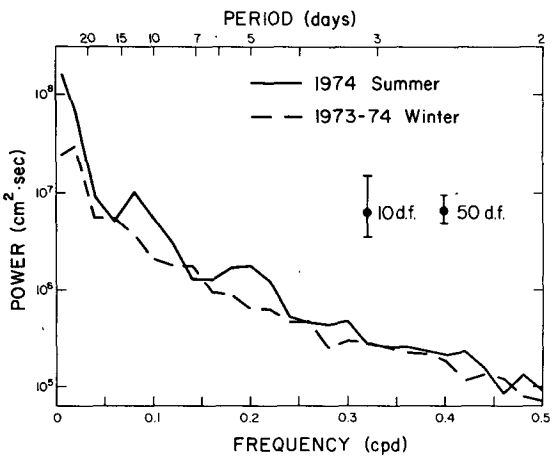

FIG. 8. Autospectra for the 1974 summer and the 1973–74 winter, each composited from individual spectra at five stations from Acapulco to Guaymas. The 90% confidence intervals corresponding to 10 and 50 df are shown (see discussion in text).

[2] It is recognized that frequency-averaging must be done with care when appreciable changes in phase occur over the averaging range. The mean change in phase across the three bands (due to the propagation) is about 45 deg. Comparison with similar plots for the individual bands indicates that the frequency-averaged index in Fig. 10 is somewhat lower than for the case of a smaller phase change, but both the alongshore variations and the differences between seasons are preserved.

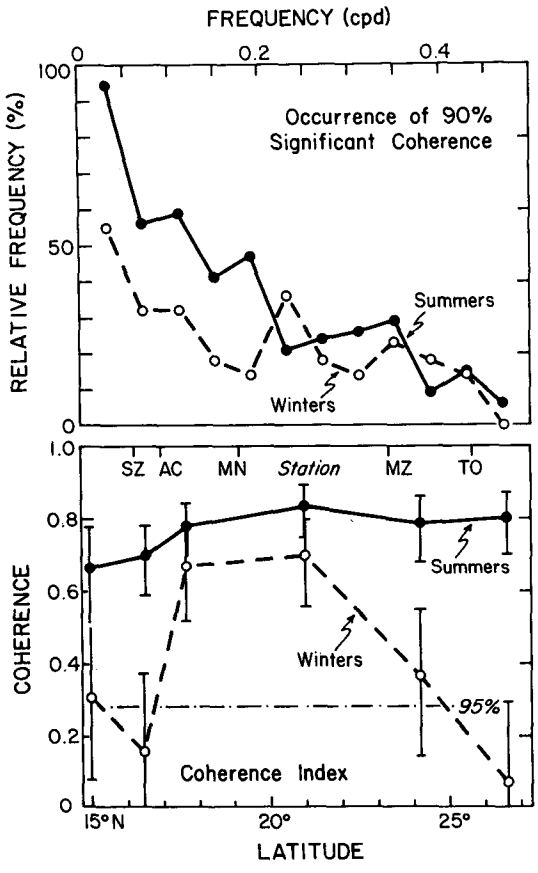

FIG. 10. Upper panel: occurrence of 90% significant coherence between stations separated by 1000 km or less, for four summers (1971, 1973–75) and two winters (1973–74, 1974–75). Bottom panel: coherence index (see text) over the 0.02–0.13 cpd band for the 1973–75 summers and winters. Vertical bars are 95% confidence intervals.

coherence are greatest and seasonal contrasts are large. The resulting index of alongshore coherence is shown as a function of location along the coast for summers and winters in Fig. 10 (lower panel).

The alongshore coherence of sea level at low frequencies is very different in summer than in winter (Fig. 10). In summer, coherence is high and significant over all the stations studied. In winter, coherences are lower than in summer at all stations, with high values only between Acapulco and Mazatlan.

The alongshore structure is interesting in that summer coherences north of Acapulco are higher and uniform. The lower summer coherence in the extreme south could be due to the less frequent forcing of propagating sea level events by storms, as suggested by the event analyses of Sections 3 and 4. On the other hand, the lack of coherent sea level activity south of Acapulco in winter is remarkable in view of the extremely energetic northerly winds that occur at Salina Cruz during that season. This is consistent with the results of the event and forcing analyses, namely, that the winter sea level events of depression at Salina Cruz do not appear to propagate as do the summer events of elevation.

c. *Propagation from phase spectra*

The phase spectrum shown in Fig. 9 is fairly typical for the summer cross spectra, with phase varying linearly with frequency. The propagation speed was determined from the phase spectrum by weighted linear regression with a zero intercept constraint (Draper and Smith, 1966, section 2.11). In conventional (unweighted) regression applications it is assumed that the variance of the dependent variable does not change over the range of the independent variable. However, at the j-th frequency band of a cross spectrum the variance of the smoothed phase estimator, F_j, is $V(F_j) = C(1 - K_j^2)/K_j^2$, where K_j is the corresponding coherence estimate and C is a constant related to the smoothing algorithm and series length (Jenkins and Watts, 1969, section 9.2). Hence, as the coherence increases (decreases), the expected variance of the phase estimate decreases (increases). The appropriate weighting scheme requires that each phase value enter the regression procedure with a weight that is inversely proportional to $V(F_j)$. This means that the j-th phase estimate is weighted according to the proportion of signal variance-to-noise variance in that frequency band. Phase estimates were used when the coherences were significant at or above the 80% confidence level, since even at this level the phase tends to follow the same pattern as those with higher coherence, but with more scatter. Because the coherences are generally higher and more frequently significant at low frequencies, the weighted regression estimates of phase speed have a low-frequency bias, and for strict interpretation should be treated accordingly.

An example of a fitted phase line is shown in Fig. 9 (lower panel). The phase estimates at the three highest frequencies failed to meet the 80% significance criterion, and were not used. The propagation speed is computed as a constant times the ratio of the station separation to the slope of the phase line. The ±95% confidence limits for the speed can be similarly found by determining the corresponding confidence interval for the slope of the regression line (Draper and Smith, 1966, section 2.11). This procedure was carried out for the 1971 summer cross spectra and for the ensemble-averaged cross spectra for the 1973–75 summers and winters. Fewer phase estimates are available for the winter spectra, and some had to be rejected because of ambiguity (between neighboring phase cycles). Low coherence made estimation of winter propagation speeds impossible for four of the station pairs. The results for the 1971 summer are shown together with the speeds found from the event analysis (Table 3) in the upper panel of Fig. 11; the

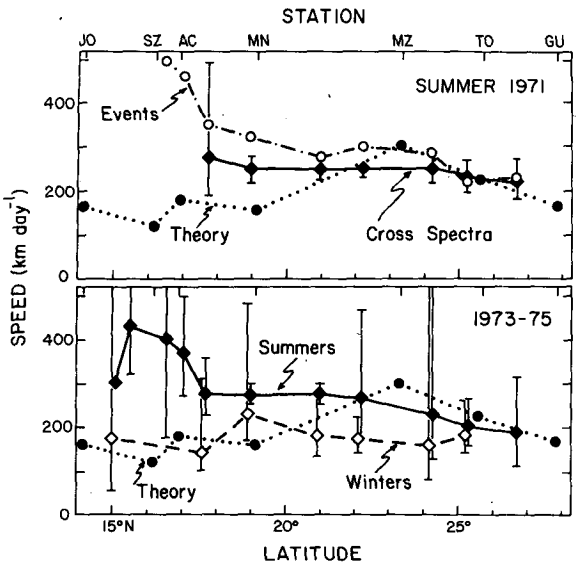

FIG. 11. Propagation speeds for the 1971 summer (upper panel) and for 1973–75 (lower panel), derived from the large-amplitude event analysis, cross-spectra (ensemble-averaged for 1973–75) and from linear, free coastal trapped wave theory for the first mode in the long wave nondispersive limit (summer stratification).

speeds for the ensemble-averaged summers and winters (1973–75) are shown in the lower panel.

In the comparison of observations with theory (Section 7), the question of dispersion is important. With few exceptions, summer phase estimates fall close to their regression line, regardless of frequency, when the corresponding coherence estimate is significant at the 90% confidence level. Enough of these estimates occur at frequencies below 0.37 cpd to say that phase speed is independent of frequency in that range (i.e., nondispersive). At higher frequencies we cannot be sure, but the few estimates that exist do not suggest any dispersion.

A number of propagation characteristics can be seen in Fig. 11. The propagation speeds found from spectral analysis are in general agreement with those found from lagged correlations (Appendix B) and the event analysis (Section 3): the overall speed magnitudes determined by the various methods are similar, winter speeds are smaller than summer speeds and summer speeds are greater in the southern region where storm forcing is ubiquitous. We note, however, that the alongshore variation of propagation speeds determined from our correlation analysis (Appendix B) tends to show relatively large summer speeds between Mazatlan and Guaymas that are not seen in the spectral analysis nor in the event analysis. These larger speeds are also found in the correlation results of Christensen *et al.* (1983). A possible explanation of this feature is that speeds based on correlations may be more affected by nonpropagative and incoherent variability than those based on cross spectra.

6. Comparison with linear theory

The summer propagative phenomena along the Mexican coast, dominated by the energetic, storm-generated events, may be thought of as undergoing two successive stages: one of generation and forced propagation followed by another of free propagation. We wish to see how well the observed propagation can be explained by the existing theory of linear free coastal-trapped waves (CTWs). The CTW models that are most appropriate for comparison with observations are those that use continuous stratification and realistic bottom topography (e.g., Wang and Mooers, 1976; Clarke, 1977; Huthnance, 1978; Brink, 1982).

Our approach to the comparison is straightforward: we explore the extent to which the observed wave speeds conform to those of linear free CTW theory in the forced and free regions. If the theory is appropriate, we may see discrepancies in the region of forcing because of the differences in propagation speeds of forced and free waves, but we expect to see a reasonable agreement in the free wave region (the existing wind data is inadequate to deal directly with the problem of forcing). Only propagation speeds can be used as a basis for comparison, as there are no observations of the current and density fields available. However, if the observed speeds in the region of free propagation are consistent with theory, we can examine the model fields of alongshore current and other diagnostic properties in order to understand the probable character of the propagation. The possible importance of nonlinear effects is discussed in Appendix C.

a. Theoretical framework

The generalized CTW is supported by both stratification and bottom topography, and the relative importance of the two effects to the free wave dynamics is controlled by the relative magnitudes of the shelf-slope width, Δ_x and the internal Rossby radius of deformation, δ_R. The importance of comparing these scales was noted by Allen (1975) for mid-latitude coastal trapped waves, and later by Huthnance (1978), Allen and Romea (1980) and Brink (1982) for generalized waves at all latitudes. At sufficiently low latitudes, Δ_x is small compared to δ_R, stratification dominates, and the wave properties are more like those of an internal Kelvin wave (IKW). This case corresponds to large values (e.g., >4) of the scale ratio $S = (\delta_R/\Delta_x)^2$, where $\delta_R = c_k/f$, f is the Coriolis parameter and c_k is the first mode internal gravity wave speed for the deep ocean. At sufficiently high latitudes (e.g., where $S < 0.25$) the opposite holds, i.e., topographic control is relatively important and the wave has properties more nearly like those of an idealized barotropic continental shelf wave (CSW).

Brink (1982) discusses the variation of CTW phase

speed with latitude as brought out in his model. Fig. 12 shows his latitudinal distributions of first mode phase speeds for CTWs (c_h), IKWs (c_k), and barotropic CSWs (c_b). Topography and stratification are fixed at representative values for the Peru coast. We have added the corresponding variation of the scale ratio S. Very close to the equator, δ_R is so large that the continental margin is of no consequence, and the phase speed of the first mode CTW, c_h, should asymptote to the local value of c_k. At low latitudes, but more poleward, the waves still resemble IKWs but Brink finds that $c_h < c_k$. He attributes this to the effect of the continental margin, where the local long internal gravity wave speed is decreased due to the smaller bottom depths; hence, "the wave 'feels' a cross-shelf, weighted average of local gravity wave speeds". Farther poleward δ_R and Δ_x are comparable (approximately, $0.25 < S < 4$), and c_h increases relative to c_k due to the transition to topographically supported waves. Finally, at high latitudes ($S < 0.25$) the waves become predominantly barotropic, and c_h surpasses the local value of c_k and continues to increase poleward. At all latitudes, $c_h > c_b$, but the two converge as latitude increases.

Fig. 12 shows that, at the latitudes of the Peru coast (4–17°S), CTWs should be like IKWs in the north and transform into a transitional, hybrid form farther south (Allen and Romea, 1980). For the latitudes of our study (13–28°N), the variation of the scale parameter in Fig. 12 suggests that CTWs should be transitional (hybrid) in the south and become more like barotropic CSWs in the north. However, Fig. 12 cannot predict the detailed behavior of hybrid free wave

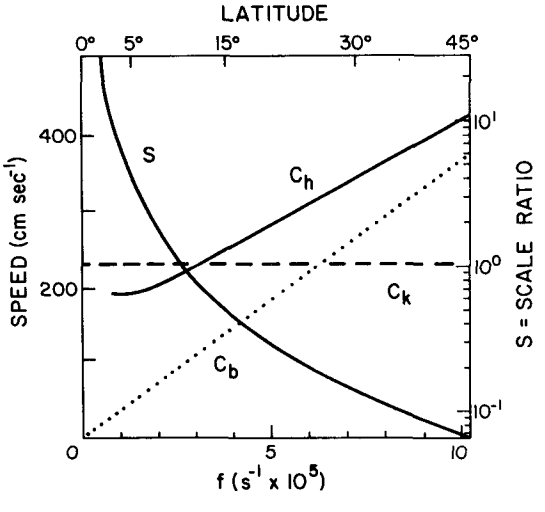

FIG. 12. Phase speed, as a function of Coriolis parameter and latitude, for first mode, free, hybrid coastal trapped long waves (c_h), internal gravity (Kelvin) waves (c_k) and barotropic continental shelf waves (c_s) (from Brink, 1982). Stratification and coastal bottom topography are fixed. Also shown is the corresponding variation of the scale parameter S discussed in the text (Section 6).

speeds for the coast of Mexico, where stratification and topography vary in a complicated manner.

To determine the theoretically expected wave characteristics for the Mexican coast during the summer season, we first found continuous profiles of squared Brunt-Väisälä frequency $N^2(z)$ with depth z (positive downward) and of bottom depth $H(x)$ with offshore distance x (positive eastward) for seven sections of coastline, each centered at one of the sea level stations from Guaymas to San Jose (Fig. 1). A representative $N^2(z)$ profile for each section was found by averaging summer hydrographic profiles (Scripps Institution of Oceanography, 1962, 1963, 1965a and 1965b) and CTD profiles (EASTROPAC, provided by M. Tsuchiya). Each profile is determined uniquely for the top 200 m from stations within the corresponding section, and for the 200–500 m layer from a common average of deep stations in all sections. From 500 m downward we assume $N^2(z) = N^2(500) \exp[(500 - z)/z_d]$, where to fit the data, $z_d = 1200$ m.

The $H(x)$ profile for each section is the average of 5–6 individual profiles extracted from high resolution (contour interval = 100 m) bathymetric worksheets, compiled by the geophysics group at Oregon State University. The offshore limit of the $(x - z)$ grid was fixed at 250 km for the San Jose section, at 200 km from Salina Cruz to Mazatlan, and at the east coast of Baja California for Topolobampo and Guaymas. The Baja California bottom topography is included in $H(x)$ for the latter two sections, while for all others a flat ocean bottom is assumed beyond the continental slope. For each section, the $N^2(z)$ and $H(x)$ profiles were used to compute the local values of c_k and c_b, respectively.

To compute the generalized CTW properties, such as c_h, alongshore velocity structures and various diagnostic parameters, we used the numerical model developed by Brink (1982). The model is linear, inviscid and unforced, with constant rotation, and uses continuous stratification and realistic bottom topography as input (the $N^2(z)$ and $H(x)$ profiles). The model is similar to those of Wang and Mooers (1976) and Huthnance (1978). The dynamical equations are solved as a two-dimensional eigenvalue problem, where to find the long wave speed a suitably low value of the alongshore wavenumber (here, 10^{-6} m^{-1}) is specified, and modal frequencies (eigenvalues) and offshore pressure–velocity structures (eigenfunctions) are computed. A particularly useful diagnostic parameter is the ratio of kinetic energy to potential energy, $R = KE/PE$ (energies integrated over the x–z grid), which is of order one at the IKW limit and large (e.g., $R > 4$) for predominantly barotropic conditions.

The theoretical long wave characteristics for summer are summarized in Table 6 for the seven sections of coastline shown in Fig. 1. The hybrid wave speeds are also plotted in Fig. 11 for comparison with the

TABLE 6. First-mode free long-wave speeds and related parameters for summer conditions along the mainland coast of Mexico, from three theories: (a) barotropic continental shelf waves, c_b; (b) long internal gravity waves for continuous stratification and a vertical wall, c_k; and (c) hybrid coastal trapped waves, c_h, from a model by Brink (1982). Included are the bottom-surface density contrast, $\Delta\sigma_t$, the total water depth (meters), the shelf-slope width given by the offshore distance to the flat ocean bottom, Δ_x, and two diagnostic parameters: a scale ratio, S, and the ratio of kinetic to potential energy, KE/PE (see text discussion).

Section	Mean latitude	$f \times 10^5$ (s^{-1})	$\Delta\sigma_t$ ($\times 10^3$)	Bottom depth (m)	Δ_x (km)	c_b	c_k (km day^{-1})	c_h	S	KE/PE
GU	27.4	6.7	5.4	1920	85	87	173	175	0.12	2.1
TO	24.8	6.1	5.6	2600	95	138	192	235	0.15	4.3
MZ	22.2	5.5	5.6	2500	125	212	187	301	0.10	5.0
MN	18.9	4.7	6.0	2800	50	49	200	160	0.97	1.9
AC	17.2	4.3	6.3	3000	50	60	206	187	1.23	2.2
SZ	15.6	3.9	6.3	3000	50	48	193	136	1.31	3.7
JO	13.9	3.5	6.6	3300	120	156	195	167	0.29	3.1

observations. Both the deep ocean bottom depth and the stratification (represented by the bottom-surface density contrast, $\Delta\sigma_t$) decrease northwestward into the Gulf of California. These changes result in a corresponding decrease of the long internal gravity wave speed from 193–206 km day^{-1} south of 20°N to 173–192 km day^{-1} north of there. The barotropic speeds (c_b) reflect changes in the topography of the continental margin, and in latitude, the former having the greatest effect. The speeds are smallest from Manzanillo to Salina Cruz, where the transition to deep ocean is very abrupt (Fig. 1), and they reach a maximum at Mazatlan where the shelf-slope width is greatest.

The first mode results from the hybrid CTW model runs (c_h, KE/PE) are in substantial agreement with expectations from the independently determined scale ratio S and barotropic and internal gravity wave speeds (c_b and c_k). Values of the scale ratio indicate that between 15°N and 20°N, coastal trapped waves should be transitional in character, whereas they should be predominantly barotropic north of 20°N, especially at Mazatlan. Accordingly, the largest speeds computed by the hybrid CTW model (c_h) are found at Mazatlan and Topolobampo, which also show the largest kinetic to potential energy ratios. The next largest value of KE/PE occurs at San Jose, which has a wide shelf (but at a lower latitude than Mazatlan) and a relatively small S value. Comparing Table 6 and Fig. 12 we see that $c_h < c_k$ in the transitional region (SZ–MN) and that—consistent with proofs given by Clarke (1977) and Huthnance (1978)—$c_h > c_b$ everywhere. Also, the only instance where $c_b > c_k$ occurs at Mazatlan, which has the widest shelf and the smallest value of S. Note that north of 20°N the combined poleward decreases in stratification, deep ocean bottom depth and shelf-slope width result in a poleward decrease in the hybrid wave speed, in spite of the increasing latitude.

To determine how well the wave speeds are resolved by the hybrid model, we have tested its response to changes in topography, stratification and grid configuration. A 50-km difference in the choice of the offshore limit of the x–z grid results in changes of 0–11% in c_h. If the Baja California "west wall" is replaced by a flat ocean bottom to 200 km at Guaymas and Topolobampo, c_h increases by 16%. If the $N^2(z)$ profile is reduced by 40% at all depths, there results a 12% reduction in c_h at Acapulco, but only 6% at Mazatlan, where the waves are more barotropic. Other experiments, in which the N^2 decrease was confined to specified depth intervals, show that 50–70% of the above speed differences are due to the stratification change below 500 m, even though the latter is numerically much smaller than the corresponding change in the upper 500 m. We conclude that care must be exercised in specifying both topography and stratification when comparing the results with observed speeds. In particular, 1) the topographic effect of the Baja peninsula should be included, 2) observed, rather than analytical, $N^2(z)$ profiles should be used and 3) realistic deep stratification should be included.

b. *Comparison with observations*

North of 20°N the observed summer wave speeds from the event and statistical analyses are consistent with those of free, hybrid coastal trapped waves as represented by the model results (Fig. 11). The differences are within the resolution of both the data and the model. The poleward decrease in c_h north of Mazatlan is well resolved by the model and observations point to the same feature, hence it is probably real. It may be attributed primarily to the (poleward) decreasing offshore scale of the mainland continental margin, and the increasing influence of the Baja California bottom topography.

In contrast, the observed summer speeds south of 20°N are significantly larger than predicted by the free CTW theory. This is consistent with indications from storm tracks and wind data (Section 3) that the storm forcing is much more prevalent in the southern zone than farther north, and generally travels poleward at large and variable speeds, consistent with those found for sea level fluctuations. The largest dis-

crepancy between observed and model speeds are in the Salina Cruz–Acapulco region, where near-coastal summer storms are most common. From Acapulco to Manzanillo the speeds as determined both from events and from cross spectra decrease to values smaller than the typical storm speeds (Table 2), but still appreciably greater than those predicted by free CTW theory. On the one hand, this seems consistent with indications from storm climatology that a fair percentage of storms leave the coastal area poleward of Acapulco (hence, the sea level propagation statistics should reflect a mixture of free and forced wave celerities). On the other hand, it may be easily shown (Appendix D) that, for forcing of the type found off of southern Mexico, a forced event should appear to propagate at a speed between that of the storm and that of the corresponding free wave.

In the region poleward of 20°N, where the disturbances appear to propagate freely, the observed wave speeds are consistent with those of first-mode coastal-trapped waves as computed by the Brink (1982) model. Second or higher modes are unlikely because they would be at least 40% slower than the observed speeds (see, e.g., Brink's Fig. 2). However, a definitive statement about the modal character of the waves cannot be made without time series measurements of the fields of velocity and mass in the x–z plane. While we cannot eliminate the possibility of higher modes, we feel that the first mode is likely to be dominant.

In general, because of the effects of stratification, hybrid CTW's remain nearly nondispersive over a greater frequency range than do barotropic shelf waves (see, e.g., Brink, 1982). To assess the variation of wave speed with frequency for the first mode CTW at Mazatlan, Topolobampo and Guaymas, c_h was calculated also for wavenumbers corresponding to frequencies near 0.35 and 0.50 cpd. The resulting values of c_h at frequencies near 0.04, 0.35 and 0.50 cpd are 301, 283, 264 km day^{-1} at Mazatlan, 233, 223, 214 km day^{-1} at Topolobampo and 171, 163, 156 km day^{-1} at Guaymas. Thus, the largest fractional change in wave speed is at Mazatlan (0.06 and 0.12), as might be expected since the wave modes there are more nearly barotropic, but the changes are generally small, especially between 0.04 and 0.35 cpd. Hence, the nondispersive nature of the sea level phase spectra (Section 6) are consistent with expectations based on the CTW model.

c. *Offshore structure of alongshore velocity*

The first mode distributions of alongshore velocity found from the inviscid Brink (1982) model for the sections off Guaymas, Topolobampo and Mazatlan, using the summer $N^2(z)$ profiles, are shown in Fig. 13. The velocities have been scaled to a sea level perturbation of 10 cm at the coast ($x = 0$, $z = 0$). The

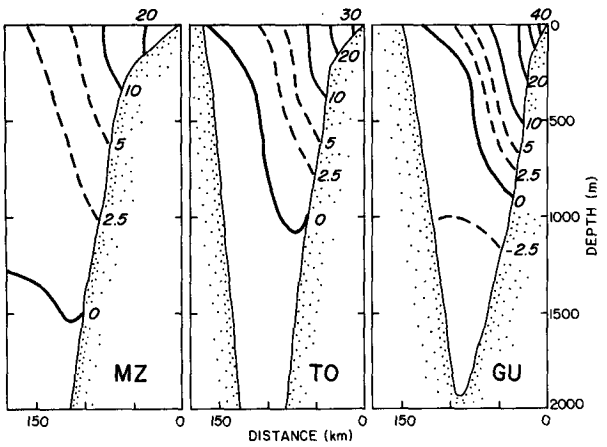

FIG. 13. Offshore structures of alongshore velocity fluctuations (cm s^{-1}) associated with first mode, free, hybrid coastal trapped waves at three stations in the Gulf of California. The distributions were computed using Brink's (1982) inviscid numerical model with realistic bottom topography (as shown) and continuous stratification (summer conditions). Magnitudes are based on a 10-cm sea level perturbation at the coast.

waves are clearly hybrid, because the isotachs are quasivertical over the shelf, as in a barotropic CSW, and slanted over the slope, reflecting a baroclinic component. Near mid-slope, at depths of 1000–1500 m, the zero isotach tends to be horizontal, as in an internal Kelvin wave. The offshore decay scale appears to be the order of ⅓–½ of the Gulf width. Brink found similar modal structures near 15°S on the Peru coast, which compared reasonably well with current observations over the slope and at mid-depth over the shelf, but not near the bottom or surface, where frictional effects are important.

d. *Seasonal changes*

The observed propagation speeds for winter conditions, as determined from cross-spectral analysis (Section 5) and crosscorrelation analysis (Christensen *et al.* (1983) and Appendix B) are generally lower than summer speeds, a feature that is probably real. This is especially true in the south, where the large speeds associated with summer storms are entirely absent in winter. Winter estimates are less reliable due to poor alongshore coherence, while north of Topolobampo they could not be determined. Hence, alongshore variations in general, and the poleward decrease in speed north of Mazatlan in particular, are unresolved by the winter data.

To see if seasonal changes in stratification explain the generally lower winter speeds, the hybrid CTW model was run with winter $N^2(z)$ profiles. In the northern region, where winter stratification is much weaker (Roden, 1964, 1972), the model speeds decrease by the smallest amounts at Mazatlan (1%), where conditions are most barotropic, and by 4% and

8%, respectively, at Topolobampo and Guaymas. Changes in c_h in the south were insignificant because the seasonality of stratification is small there. Thus, the model does not predict seasonal variations in c_h that would be detectable through observations. In winter, observed and model speeds in the southern region are very similar, suggesting that the propagating variability there may be predominantly unforced. This is consistent with the lack of tropical storm activity in winter and the low correlation of the Acapulco winds with local sea level (Table 5). The linear CTW model cannot account for the lower speeds observed in winter near Mazatlan.

7. Summary

To summarize, we find:

1) Large-amplitude, propagating events of elevation (10–30 cm) occur intermittently during the summer, and are associated with eastern North Pacific tropical storms, whose centers pass within 500 km of the southern coast of Mexico (Salina Cruz to Manzanillo). The storms usually move poleward parallel to the coastline at high speeds (400–600 km day^{-1}), eventually turning westward toward the open Pacific north of 20°N. This and the occurrence of large maximum daily winds at Acapulco during storm passages, suggest that the sea level events are usually forced disturbances south of 20°N and freely propagating north of there. The lack of tropical storms and large-amplitude sea level events in winter probably accounts for the lower sea level coherence and slower propagation speeds observed in that season.

2) In summer, both the Acapulco wind and the Guaymas wind are locally correlated with sea level (the Acapulco wind more highly), but uncorrelated with each other. The correlation of the Acapulco wind and the non-correlation of the Guaymas wind with remote sea level, and the lags of maximum correlation, indicate that propagating sea level variability is forced by the Acapulco wind but not by the wind as far north as Guaymas. In winter, high correlations between Salina Cruz sea level and local wind represent the association between energetic events of depression in sea level, and strong northerly (offshore) winds over the Gulf of Tehuantepec. There are no visual or statistical indications that this variability propagates poleward from Salina Cruz.

3) In a multiple-input statistical model of sea level forcing at Salina Cruz, Acapulco and Guaymas, the propagation process (represented by remote sea level) contributes the most to the summer variability of adjusted sea level at all stations. This is followed by local wind (Acapulco and Guaymas), while large scale atmospheric pressure variability is unimportant. In winter at Salina Cruz the local wind contributes the most, followed by sea level to the south, but neither contributes to sea level variability at Acapulco and Guaymas.

4) There is generally high coherence in coastal sea level from San Jose (14°N) to Guaymas (28°N) during the summer–fall season (May–October). Significant coherence values occur often at frequencies from 0.02 to 0.13 cpd, and sporadically at frequencies above 0.21 cpd. Coherence tends to be lower and less frequently significant south of Acapulco.

5) Summer phase spectra indicate alongshore propagation speeds that are high south of 20°N (250–500 km day^{-1}), and lower to the north (180–300 km day^{-1}). The latter show a tendency to decrease poleward from Mazatlan (250–300 km day^{-1}) to Guaymas (180–230 km day^{-1}). Phase varies linearly with frequency at least to 0.37 cpd, indicating that the disturbances propagate nondispersively.

6) Alongshore coherence during winter (November–April) is generally lower and less frequently significant than in summer at frequencies below 0.21 cpd. Winter coherence at low frequencies (0.02–0.13 cpd) is highest between Acapulco (17°N) and Mazatlan (23°N), and low elsewhere. Winter propagation speeds are slower and more uniform than those of summer (140–230 km day^{-1}); the slower propagation is especially notable in the south, where the high summer speeds are absent, consistent with the absence of tropical storm forcing in winter.

7) An inviscid, linear numerical model of free coastal-trapped waves, based on realistic bottom topography and continuous stratification (Brink, 1982), indicates that freely propagating long waves along the Mexican coast should be of the hybrid type, with a barotropic structure over the shelf and a baroclinic structure farther offshore. In the southern region (narrow shelf) the predicted free wave speeds are approximately half those observed, consistent with the expected effects of the forcing observed there. North of 20°N (wider shelf), the predicted speeds are similar in magnitude to those observed and replicate the observed poleward decrease from Mazatlan to Guaymas. The observed nondispersive nature of the propagation over the frequencies 0.04–0.35 cpd is consistent with the calculated first-mode coastal-trapped waves. Based on the amplitudes of large events and on model estimates of the associated alongshore currents, it appears that (Appendix C) nonlinear effects may occur during energetic events of elevation, but that their detection by this data set is difficult.

Acknowledgments. We thank the Centro de Investigacion Cientifica y de Ensenāza Superior de Ensenada (CICESE), in particular, Drs. Niels Christensen, Jr. and Antoine Badan-Dangon, for their invaluable assistance in obtaining data on sea level, atmospheric pressure and winds for the coast of Mexico. We are indebted to Dr. Kenneth Brink, for making his numerical model available to us, and for his valuable discussions. Special thanks are due to Dr. David Birkes for his assistance in statistical matters. The

thoughtful comments of two anonymous reviewers are greatly appreciated. This research was supported by the National Science Foundation under Grants OCE 78-26820, OCE 80-17929, OCE 80-24116 and OCE 80-14939. A substantial fraction of the computer resources were provided under a grant from the Oregon State University Computer Center.

APPENDIX A

Dominant Wind Forcing

According to Garrett and Toulany (1982), the direction of dominant forcing of a scalar time series, $h(t)$, by a vector time series $U(t)$, $V(t)$, may be defined as the direction θ_d in which the wind must blow to produce a maximum response. In practice, θ_d may be found by performing the multiple regression $h(t) = aU(t) + bV(t) + \text{noise}$, whence $\theta_d = \tan^{-1}(b/a)$. This is equivalent to finding the direction in which the vector component is best correlated with the scalar response. The corresponding correlation (C_d), and the dominant forcing direction (θ_d) are then given by

$$C_d = (C_1 + C_2T)(1 + 2CT + T^2)^{-1/2}, \quad \text{(A1)}$$

$$\theta_d = \tan^{-1}[T(S_u/S_v)], \quad \text{(A2)}$$

where $T = (C_2 - CC_1)/(C_1 - CC_2)$, S_u and S_v are the standard deviations of U and V, and C_1, C_2, and C are the correlation coefficients for the bivariate pairs (h, U), (h, V) and (U, V), respectively.

Other methods exist for representing the effects of a vector-valued time series by using one of its (scalar) components. One is simply to resolve the vectors in the principal axis direction (i.e., that of the first empirical eigenvector). Another is to take components in the direction of the inner phase, as computed in a complex correlation analysis (Mooers, 1973). The inner phase α_I between a scalar and a vector time series (sea level and wind, here) reduces to

$$\alpha_I = \tan^{-1}[C_2/C_1]. \quad \text{(A3)}$$

All three approaches (dominant forcing, principal axis and inner phase) were applied to the Guaymas and Acapulco wind data for the various station/seasons. Such analyses are obviated for Salina Cruz, where winds are never reported as being from any direction except north or south.

The correlation corresponding to dominant forcing C_d is moderate for the 1974 and 1975 summers at Guaymas (0.278, 0.287) and Acapulco (0.314, 0.344). All winter values of C_d at these stations were less than 0.1. For cases where C_d is statistically significant, all three measures of direction (dominant forcing, principal axes and inner phase) indicate that a rise in sea level is forced most efficiently by wind from the southeast and east octants, respectively, at Guaymas and Acapulco. At Guaymas the dominant forcing direction corresponds closely to the directional trend of the coastline, and at Acapulco it is only 15–20 degrees away from the coastline trend. For low values of C_d, the principal axis still implies these directions. At Salina Cruz, sea level rises are always associated with southerly (onshore) winds, showing moderate forcing in the 1973 and 1974 summers (C_2 = 0.256, 0.279) and strong forcing in the two winters (C_2 = 0.543, 0.659).

APPENDIX B

Propagation From Correlation Analysis

As an overall measure of coherence and propagation over a wide range of frequencies, we computed the maximum lagged crosscorrelations and the propagation speeds implied by their lags.[3] These are shown in Table B1 for the 1971 and 1974 summers and the 1973–74 winter. The summer of 1971 is included (even though the 1971 data are unadjusted for the atmospheric pressure) for comparison with the propagation statistics of individual events in that year (Section 3). Note that, because overlapping station pairs were analyzed, the statistics for adjacent rows in Table B1 are not independent of each other, though those for alternate rows are.

If the mean correlation magnitude is computed for all seven station pairs from GU–TO to MN–AC for each summer (S) and winter (W) season, the overall correlations are ranked as follows: S-1971 (0.844), S-1974 (0.774), S-1973 (0.676), W-1973/74 (0.522) and W-1974/75 (0.505). The differences between summers and winters are probably real and can be readily explained by the non-occurrence of large-amplitude, coherent events during the winters. Insignificant correlations occur in winter, and station pairs involving Salina Cruz and San Jose are more poorly correlated than those farther north in both seasons. Both these features are replicated for the winter and summer seasons not shown in Table B1.

Care is needed in comparing statistics for 1971 with those for 1973–75, because the 1971 data were not adjusted for atmospheric pressure. To estimate the impact of the barometric contribution to the 1971 correlations, we recomputed the lagged correlations for the 1974 summer using unadjusted data. The averaged correlations for the adjusted data (Table B1) were only 3.5% lower than for the unadjusted data. On the other hand, the adjusted (unadjusted) 1974 summer data had maximum correlations about 8% (5%) lower than for 1971. Hence, the effect of adjustment is small, and the 1971 summer should probably still be ranked first. The strength of the 1971 summer correlations probably reflects the greater

[3] The significance levels for all correlations were found by first determining the effective degrees of freedom after accounting for persistence in the data, consistent with Davis (1976) and Sciremammano (1979).

TABLE B1. Station pairs, separations, maximum lagged correlations (r_{max}), propagation speeds (c) and estimated speed uncertainties (Δc) for selected seasons. Correlations significant at the 95% confidence level or better are in boldface. All propagation speeds are in the poleward sense. Speeds are not calculated for nil lags or where the correlation is not significant at the 95% confidence level. Entries are left blank for the southernmost stations in the 1971 summer, due to a lack of data.

Station pair	Separation (km)	Summer 1971			Summer 1974			Winter 1973–74		
		r_{max}	c (km day^{-1})	Δc (km day^{-1})	r_{max}	c (km day^{-1})	Δc (km day^{-1})	r_{max}	c (km day^{-1})	Δc (km day^{-1})
GU–TO	320	**0.92**	254	100	**0.79**	318	160	**0.70**	—	—
GU–MZ	670	**0.85**	245	50	**0.78**	225	40	**0.50**	135	30
TO–MZ	360	**0.92**	285	110	**0.74**	356	180	**0.55**	119	40
TO–MN	920	**0.82**	263	40	**0.76**	460	120	0.31	—	—
MZ–MN	560	**0.86**	251	60	**0.84**	282	70	**0.57**	—	—
MZ–AC	1090	**0.71**	274	30	**0.75**	274	30	**0.41**	274	70
MN–AC	530	**0.82**	265	70	**0.76**	265	70	**0.61**	133	30
MN–SZ	1080				**0.64**	359	60	−0.12	—	—
AC–SZ	550				**0.60**	548	270	−0.16	—	—
AC–JO	1070				**0.60**	269	30	−0.29	—	—
SZ–JO	530				**0.70**	263	70	**0.48**	175	60

number of tropical storms and large-amplitude events that occurred in that year.

A rational discussion of propagation requires some consideration of the uncertainties inherent in the determination of the propagation speeds. Unfortunately, we know of no systematic method for estimating the uncertainty in lags found from maximum lagged crosscorrelations. Comparison of the lags for the same seasons and station pairs but for different years yields mean interannual lag differences of three observation intervals (18 h) for summer and six intervals (36 h) for winter. These are probably upper limits on the lag uncertainty, since part of the differences could be real. For the purposes of discussion we assume that lag uncertainties of two and four observation intervals are reasonable estimates for the summer and winter seasons, respectively, as a basis for computing speed uncertainties. For a postulated lag uncertainty, $\Delta\lambda$, the corresponding speed uncertainty may be expressed as $\Delta c = D/2[(\lambda - \Delta\lambda)^{-1} + (\lambda + \Delta\lambda)^{-1}]$, where D is the station separation and λ is the estimated lag. For our estimates of λ and $\Delta\lambda$, $\Delta\lambda/\lambda$ ranges from 0.2 to 0.5. Consequently, assuming $(\Delta\lambda/\lambda) < 1$ we obtain $\Delta c = c(\Delta\lambda/\lambda + O[\Delta\lambda/\lambda]^3)$, where $c = D/\lambda$. Thus, $\Delta c \approx c^2\Delta\lambda/D$ and for a typical summer case (Table B1) where $D = 500$ km, $c = 280$ km day^{-1}, and $\Delta\lambda = 12$ h the speed uncertainty would be 80 km day^{-1}. The speed uncertainties thus calculated are shown in Table B1 along with the correlations and estimated speeds. Note that, in spite of the lower correlation magnitudes in winter, speed uncertainties are generally smaller because the lags (λ) are larger.

Based on our assumptions about lag uncertainties, the correlation results, in general, indicate significant differences between seasons, but consistency between years. Maximum correlations from 0.6 to 0.8 are typical of the summers, and less than 0.6 for winters. In the summer of 1971, most of the propagation speeds fall in the range of 200–300 km day^{-1}, agreeing generally with those found in the event analysis (Section 3) and in the spectral analysis (Section 5). Large summer speeds are found between Acapulco and Salina Cruz, also in agreement with the other analyses and with indications of storm forcing there. The propagation speeds from winter correlations tend to be considerably lower, typically less than 200 km day^{-1}.

While the overall speeds from the correlations are similar to those found in the spectral and event analyses, there is some lack of similarity in the alongshore distribution of the speeds. For example, there is a tendency for the summer speeds from correlations to be high north of Manzanillo, especially near Topolobampo and Mazatlan. This agrees with the correlation results of Christensen *et al.* (1983), but is not reflected in our spectral results (Fig. 11). On the other hand, in the three summers for which we have Salina Cruz data (1973–75), propagation speeds are high from Salina Cruz to Acapulco, agreeing with the spectral and event analyses as well as with indications of storm forcing in that region. Christensen *et al.* do not report high speeds in the south, but their analysis did not extend to Salina Cruz and was not seasonally stratified.

APPENDIX C

Nonlinear Effects

The energetic, storm-generated events along the coast of Mexico are of large amplitude, compared with the background variability in this region, and occur as solitary waves of elevation. For 20 events identified over four summers (1971, 1973–75), we have estimated average elevations (above the background level) of 15 cm, 16 cm, and 13 cm, with standard deviations of 6 cm, 7 cm and 5 cm at Mazatlan,

Topolobampo and Guaymas, respectively. Several of the larger sea level events are accompanied by perturbations of the order of 20 cm or more. The large amplitude nature of the events raises the question of the possible importance of nonlinear effects. Another motivation for addressing this point is the apparent inability of linear theory to account for the observed seasonal changes in propagation speed north of 20°N, where forcing is not believed to be a factor.

A nonlinear theory for generalized coastal trapped waves does not exist at the present, but, for barotropic shelf waves, theoretical models for the balance of weak nonlinear effects by topographic dispersion have been developed by Smith (1972) and Grimshaw (1977). These models indicate that for the lowest cross-shelf mode, nonlinear solitary waves with propagation velocities greater than the linear long-wave speed may exist as waves of sea level elevation, but not as waves of depression. This result stimulates additional interest in the possible importance of nonlinearity because the summer, storm induced sea level disturbances appear as isolated waves of elevation that resemble solitary waves and that propagate over large distances. In contrast, the isolated large-amplitude sea level depressions generated at Salina Cruz in the winter do not appear to propagate northward to Acapulco as nondispersive disturbances. Nonlinear effects need not be present to explain these qualitative features, however. Behavior similar to that observed in the summer could result simply from linear coastal trapped waves with wavelengths long enough to be effectively nondispersive. Also, the winter free wave propagation between Salina Cruz and Acapulco could be inhibited by increased bottom friction or by scattering due to irregularities in the stratification between those particular locations. Alternatively, the large sea level depressions at Salina Cruz in the winter could be primarily related to local effects induced by the strong, predominantly offshore winds. The possibility that nonlinear effects may be playing a role, however, merits consideration.

The lack of a directly applicable theory and of data other than coastal sea level heights makes a quantitative assessment of the importance of nonlinearities difficult, but some estimates may be made. In the theory for weakly nonlinear and weakly dispersive barotropic shelf waves (Smith, 1972; Grimshaw, 1977), the equation for the amplitude $\zeta(y, t)$ of sea level at the coast, for the lowest cross-shelf wave mode, takes the form

$$\zeta_t + (\gamma\zeta + c)\zeta_y = D(\zeta), \qquad \text{(C1)}$$

where t is time, y distance alongshore (positive northward), c the linear long wave speed, $D(\zeta)$ a linear dispersive term, $\gamma = \delta g(f\Delta_x)^{-1}$, g the acceleration due to gravity, and δ an O(1) number dependent on the cross-shelf topography and the modal structure. Since the alongshore velocity v is in geostrophic balance to lowest order, i.e., $fv = g\zeta_x$, it is clear that $\gamma\zeta$ in (C1) represents an effective alongshore velocity

$$\gamma\zeta = v_e(y, t). \qquad \text{(C2)}$$

For a given $\zeta(y, t)$, the relative importance of nonlinear effects in (C1) then may be estimated by comparing the magnitudes of v_e and c. This type of comparison follows also, of course, from a simple estimate of the relative magnitude of the linear time derivative and the nonlinear advection term in the vorticity equation. For $v_e/c \ll 1$, the propagation of waves of alongshore wavenumber l and of frequency ω will be primarily linear for changes in time $\Delta t < T_N = \omega^{-1}(c/v_e)$ (e.g., Whitman, 1974; sections 2.1, 2.8, 2.10), or corresponding propagation distances $\Delta y = c\Delta t \ll L_N$, where

$$L_N = cT_N = c(lv_e)^{-1} = c^2(\omega v_e)^{-1}. \qquad \text{(C3)}$$

Without a theoretical model that gives a formula for δ, a quantitative expression for v_e in terms of ζ is not known. We can make an estimate of the maximum value v_{em} that accompanies a typical summer sea level event in the free wave region, Mazatlan to Guaymas, by using the solutions shown in Fig. 13 for the cross-shelf structure of the alongshore velocity $v(x, z)$ from the linear hybrid wave modes, and a typical sea level elevation during these events of 15 cm. As a guide to estimating v_e from $v(x, z)$, we utilize results from the barotropic model in Grimshaw (1977). We find there that for the first shelf wave mode over an exponential slope $|v_e| \approx 0.9v_{\max}$, where $v_{\max}$ is the maximum value of $|v(x, z)|$ and where $v_{\max}$ occurs at the coast. Thus, referring to Fig. 13, we assume that for $\zeta = 10$ cm, $v_e = 25$, 30 and 35 cm s^{-1} for Mazatlan, Topolobampo, and Guaymas, respectively. For a maximum sea level elevation of $\zeta_m = 15$ cm, this gives, respectively, $v_{em} = 37.5$, 45, 52.5 cm s^{-1} and, with c_h from Table B1, $v_{em}/c_h = 0.11$, 0.17, and 0.27. These estimates indicate that $v_{em}/c_h < 1$ and thus that nonlinear effects may be weak. However, if we estimate L_N in (C3) using, for example, $v_e/c_h = 0.15$, $c_h = 250$ cm day^{-1} and $\omega = 0.1$–0.3 cpd, we obtain $L_N \approx 2650$–850 km. These values of L_N are not large compared with the propagation distances involved (e.g., 1240 km between Manzanillo and Guaymas), especially for the higher frequencies. Consequently, because of the relatively long distances over which the disturbances propagate, the estimated values of v_e/c_h are not small enough to rule out the possible importance of nonlinear effects. The estimates are certainly not precise, and all that can be fairly concluded is that it is possible that nonlinear effects play a role in the propagation of these events. More quantitative statements will have to await the development of an appropriate nonlinear model and perhaps future measurements, probably of currents, on the Mexican continental shelf.

It is worthwhile noting that if (C1) is a Korteweg–de Vries (KdV) equation (Grimshaw, 1977) or a Benjamin–Davis–Ono (BDO) equation (Smith, 1972), the solitary wave solutions have a wave speed

$$c_s = c + \Delta c_s, \tag{C4}$$

where for the KdV equation $\Delta c_s = \frac{1}{3}v_{em}$ and for the BDO equation $\Delta c_s = \frac{1}{4}v_{em}$ (e.g., Miles, 1981). Thus, if $v_{em} = 45$ cm s^{-1}, $\Delta c_s = 11$–15 cm s^{-1} and the estimated increase in solitary wave speed over the linear wave speed is generally less than 0.1 c_h and is small. As a result, with the uncertainties involved in estimating propagation velocities from observations and in obtaining appropriate wave speeds from models, it would in this case be extremely difficult to differentiate between linear, nondispersive propagation and nonlinear, solitary wave propagation based on wave speeds alone. In particular, the estimated Δc_s, if correct, is too small to account for the seasonal differences in observed propagation speeds near Mazatlan.

APPENDIX D

Sea Level Response to Storm Forcing

To provide qualitative information on expected propagation velocities of sea level fluctuations forced by tropical storms, such as those observed off Mexico in the summer (Section 3), we consider the following idealized model. It is assumed that the linear theory for forced, frictionless, hybrid coastal-trapped waves applies (e.g., Clarke, 1977). The resulting equation for the amplitude of sea level at the coast ζ, for the lowest cross-shelf mode, takes the form

$$\zeta_t + c\zeta_y = b\tau(y, t), \tag{D1}$$

where t is time, y distance alongshore (positive poleward), c the linear first mode wave speed, b a positive constant depending on the topography and modal structure, and $\tau(y, t)$ the alongshore (y) component of the wind stress at the coast.

To model the response to tropical storms of the type discussed in Section 3, we consider an initial-value problem with

$$\zeta = 0 \quad \text{at} \quad t = 0, \tag{D2}$$

$$\tau = \begin{cases} \tau_0 L_s \delta(y - c_s t), & 0 \leq y \leq L, \\ 0, & y < 0, \quad y > L. \end{cases} \tag{D3}$$

The wind stress is represented by a Dirac-delta function of strength $\tau_0 L_s$ that travels poleward along the coast in the region $0 \leq y \leq L$ with a constant velocity $c_s > c$.

The solution to (D1), with (D2) and (D3), is

$$\zeta = \begin{cases} K_2[H(y - ct) - H(y - c_s t)], & 0 \leq t \leq L/c_s, \\ K_2[H(y - ct) - H(y - K_1 - ct)], & L/c_s \leq t, \end{cases} \tag{D4}$$

where H is the Heaviside unit function, $K_1 = L(c_s - c)/c_s$, and $K_2 = b\tau_0 L_s/(c_s - c)$.

The sea level response as a function of y for $t < L/c_s$ is thus a propagating, expanding top hat function, with leading and trailing edges originating from $y = 0$ at $t = 0$ and traveling poleward at velocities c_s and c, respectively. For $t > L/c_s$, the forcing is absent and the top hat function propagates poleward as a free wave with velocity c and with constant width K_1.

In the forcing region $0 < y < L$, the apparent propagation velocity c_c of the *center* of the top hat function, determined as with the observations from time series of ζ for various y, is $c_c = \frac{1}{2}(c_s + c)$. Consequently, in the region of forcing c_c is the average of the storm speed and the free wave speed. Outside the region of forcing, i.e., for $y > L$, c_c equals the free wave speed c as expected.

REFERENCES

Allen, J. S., 1975: Coastal trapped waves in a stratified ocean. *J. Phys. Oceanogr.*, **5**, 300–325.

——, and R. D. Romea, 1980: On coastal trapped waves at low latitudes in a stratified ocean. *J. Fluid Mech.*, **98**, 555–585.

Baum, R. A., 1974: Eastern North Pacific hurricane season of 1973. *Mon. Wea. Rev.*, **102**, 296–306.

——, 1975: Eastern North Pacific tropical cyclones, 1974: Part 1. *Mon. Wea. Rev.*, **103**, 301–304.

Brink, K. H., 1982: A comparison of long coastal trapped wave theory with observations off Peru. *J. Phys. Oceanogr.*, **12**, 897–913.

Chelton, D. B., and R. E. Davis, 1982: Monthly mean sea level variability along the west coast of North America. *J. Phys. Oceanogr.*, **12**, 757–784.

Christensen, N., Jr., R. de la Paz and G. Gutierrez, 1983: A study of sub-inertial waves off the west coast of Mexico. *Deep Sea Res* (in press).

Clarke, A. J., 1977: Observational and numerical evidence for wind-forced coastal trapped long waves. *J. Phys. Oceanogr.*, **7**, 231–247.

Crutcher, H. L., and R. G. Quayle, 1974: *Mariners Worldwide Climatic Guide to Tropical Storms at Sea.* NAVAIR 50-1C-61, U.S. Government Printing Office, Washington, D.C., 54–65.

Davis, R. E., 1976: Predictability of sea surface temperature and sea surface pressure anomalies over the North Pacific Ocean. *J. Phys. Oceanogr.*, **6**, 249–266.

Denney, W. J., 1972: Eastern North Pacific hurricane season of 1971. *Mon. Wea. Rev.*, **100**, 276–293.

Draper, N. R., and H. Smith, 1966: *Applied Regression Analysis.* Wiley, 407 pp.

Enfield, D. B., and J. S. Allen, 1980: On the structure and dynamics of monthly mean sea level anomalies along the Pacific coast of North and South America. *J. Phys. Oceanogr.*, **10**, 557–578.

Garrett, C., and B. Toulany, 1982: Sea level variability due to meteorological forcing in the northeast Gulf of St. Lawrence. *J. Geophys. Res.*, **87**, 1968–1978.

Grimshaw, R., 1977: Nonlinear aspects of long shelf waves. *Geophys. Astrophys. Fluid Dyn.*, **8**, 3–16.

Gunther, E. B., 1980: Eastern north Pacific tropical cyclones of 1979. *Mon. Wea. Rev.*, **108**, 631–641.

Huthnance, J. M., 1978: On coastal trapped waves: Analysis and numerical calculation by inverse iteration. *J. Phys. Oceanogr.*, **8**, 74–92.

Jenkins, G. M., and D. G. Watts, 1969: *Spectral Analysis and its Applications.* Holden-Day, 525 pp.

Miles, J. W., 1981: The Kurteweg–de Vries equation: An historical essay. *J. Fluid Mech.*, **106,** 131–147.

Mooers, C. N. K., 1973: A technique for the cross spectrum analysis of pairs of complex-valued time series, with emphasis on properties of polarized components and rotational invariants. *Deep Sea Res.*, **20,** 1129–1141.

Riehl, H., 1954: *Tropical Meteorology.* McGraw-Hill, 281–357.

Roden, G. I., 1964: Oceanographic aspects of Gulf of California. *Marine Geology of the Gulf of California: a Symposium.* Tj. H. van Andel and G. G. Shor Jr., Eds., Amer. Assoc. Petrol. Geologists Mem., No. 3, 30–58.

——, 1972: Thermohaline structure and baroclinic flow across the Gulf of California entrance and in the Revilla Gigedo Islands region. *J. Phys. Oceanogr.*, **2,** 177–183.

Romea, R. D., and J. S. Allen, 1982: On forced coastal trapped waves at low latitudes in a stratified ocean. *J. Mar. Res.*, **40,** 369, 401.

Sciremammano, F., 1979: A suggestion for the presentation of correlations and their significance levels. *J. Phys. Oceanogr.*, **9,** 1273–1276.

Scripps Institution of Oceanography, 1962: *Oceanic Observations of the Pacific: 1955.* University of California, Berkeley and Los Angeles, University of California Press. 477 pp.

——, 1963: *Oceanic Observations of the Pacific: 1956.* Berkeley and Los Angeles, University of California Press. 458 pp.

——, 1965a: *Oceanic Observations of the Pacific: 1954.* Berkeley and Los Angeles, University of California Press. 426 pp.

——, 1965b: *Oceanic Observations of the Pacific: 1957.* Berkeley and Los Angeles, University of California Press. 707 pp.

Smith, R., 1972: Nonlinear Kelvin and continental shelf waves. *J. Fluid Mech.*, **52,** 379–391.

Smith, R. L., 1978: Poleward propagating perturbations in currents and sea levels along the Peru coast. *J. Geophys. Res.*, **83,** 6083–6092.

Snedecor, G. W., and W. G. Cochran, 1980: *Statistical Methods,* 7th ed. Iowa State University Press, 507 pp.

Thompson, W. J., and R. L. Ellsberry, 1981: An analysis of eastern North Pacific tropical cyclone forecast errors. *Mon. Wea. Rev.*, **109,** 1930–1938.

Wang, D-P., and C. N. K. Mooers, 1976: Coastal trapped waves in a continuously stratified ocean. *J. Phys. Oceanogr.*, **6,** 853–863.

Whitman, G. B., 1974: *Linear and Nonlinear Waves.* Wiley and Sons, 636 pp.